



**HAL**  
open science

# Uncertainties in short-term forecasts of a Mediterranean heavy precipitation event: Assessment with satellite observations

H. Clark, Jean-Pierre Chaboureau

► **To cite this version:**

H. Clark, Jean-Pierre Chaboureau. Uncertainties in short-term forecasts of a Mediterranean heavy precipitation event: Assessment with satellite observations. *Journal of Geophysical Research: Atmospheres*, 2010, 115, pp.D22213. 10.1029/2010JD014388 . hal-00562341

**HAL Id: hal-00562341**

**<https://hal.science/hal-00562341v1>**

Submitted on 16 Jun 2022

**HAL** is a multi-disciplinary open access archive for the deposit and dissemination of scientific research documents, whether they are published or not. The documents may come from teaching and research institutions in France or abroad, or from public or private research centers.

L'archive ouverte pluridisciplinaire **HAL**, est destinée au dépôt et à la diffusion de documents scientifiques de niveau recherche, publiés ou non, émanant des établissements d'enseignement et de recherche français ou étrangers, des laboratoires publics ou privés.

Copyright

## Uncertainties in short-term forecasts of a Mediterranean heavy precipitation event: Assessment with satellite observations

Hannah Clark<sup>1</sup> and Jean-Pierre Chaboureau<sup>1</sup>

Received 20 April 2010; revised 26 August 2010; accepted 30 August 2010; published 30 November 2010.

[1] The uncertainties in short-term forecasts of a 5 day episode of heavy precipitation in southeastern France were investigated. The episode took place from 19 to 23 November 2007 resulting in 400 mm of precipitation locally and was fairly typical of events known as “Cevenoles” that frequently affect the region. Several sets of 24 h meso-NH simulations were constructed that differed in their initial and boundary conditions. Comparison with rain gauges showed that simulations initialized from large-scale operational analyses failed to capture the intensity of precipitation associated with convective events and overestimated the amount of precipitation when the conditions were not convective. In contrast, simulations starting from the mesoscale analysis of the French operational mesoscale model ALADIN were more successful in forecasting the amount and location of the precipitation. Satellite observations revealed that this was due to a better prediction of the intensity of the surface wind over the sea during the stratiform regime and a more timely onset of convection over the sea related to a better prediction of the quantity of precipitable water. This study shows the benefits of using satellite observations to verify precipitation forecasts over the sea.

**Citation:** Clark, H., and J.-P. Chaboureau (2010), Uncertainties in short-term forecasts of a Mediterranean heavy precipitation event: Assessment with satellite observations, *J. Geophys. Res.*, 115, D22213, doi:10.1029/2010JD014388.

### 1. Introduction

[2] The Mediterranean region is frequently affected by severe weather events particularly during fall. The Mediterranean sea is a source of heat and moisture, and this aspect combined with the complex orography of the region, renders the area prone to flash floods. The high population density around the Mediterranean coastline means that such events can have a large human and economic impact. In recent years, one of the most extreme events affected Nimes (see its location in Figure 1b) and the Gard region of France, from 8 to 9 September 2002 resulting in 690 mm of precipitation in 24 h which led to 24 deaths and about 1 billion U.S. dollars of damage [Delrieu *et al.*, 2005].

[3] The Gard region is located in the southeastern part of the Massif Central or “Cevennes.” This particular area is subject to heavy precipitation events, known as “Cevenoles.” Three factors are conducive to these events (see Ducrocq *et al.* [2008] and Nuissier *et al.* [2008] for a recent review). First, a relatively warm Mediterranean Sea favors their occurrence during late summer and early fall. A second ingredient is the presence of an upper-level trough located to the west of the Cevennes [e.g., Chaboureau and Claud, 2006; Hoinka *et al.*, 2006; Funatsu *et al.*, 2008, 2009]. The upper-level trough generates a southerly flow that advects warm, moist air

masses from the Mediterranean Sea toward the coast, and is able to destabilize the air masses. A third factor is the steep orography that channels the low-level flow. This induces moisture convergence and, in the case of convective instability, contributes eventually to its release by triggering orographic convective precipitation.

[4] There have been several studies aimed at characterizing the sensitivity of Mediterranean heavy precipitation events to the aforementioned factors [e.g., Romero, 2001; Ducrocq *et al.*, 2002; Lagouvardos and Kotroni, 2005; Lebeaupin *et al.*, 2006; Argence *et al.*, 2008; Ducrocq *et al.*, 2008; Nuissier *et al.*, 2008]. Some recent articles have pointed out the inadequacy of the representation of humidity, especially over the sea, and tested the assimilation of nonconventional data to improve the quantitative precipitation forecasts [e.g., Ducrocq *et al.*, 2002; Lagouvardos and Kotroni, 2005; Faccani *et al.*, 2005]. A few studies have examined the sensitivity of the precipitation forecast to oceanic conditions [e.g., Lebeaupin *et al.*, 2006; Lebeaupin Brossier *et al.*, 2008]. It has also been shown that heavy precipitation events in the western Mediterranean are sensitive to small differences in the location, shape and intensity of the upper-level trough [Romero, 2001; Argence *et al.*, 2008, 2009].

[5] The episode of intense precipitation that we considered affected southeastern France, and in particular the Cevennes. It lasted 5 days from 19 to 23 November 2007, resulted in 400 mm of precipitation in certain areas (with a maximum of 426 mm over the hills of the Cevennes), and caused localized flooding. This episode was the wettest in the area for the year 2007. It was also a major event with respect to

<sup>1</sup>Laboratoire d’Aérodologie, Université de Toulouse, CNRS, Toulouse, France.

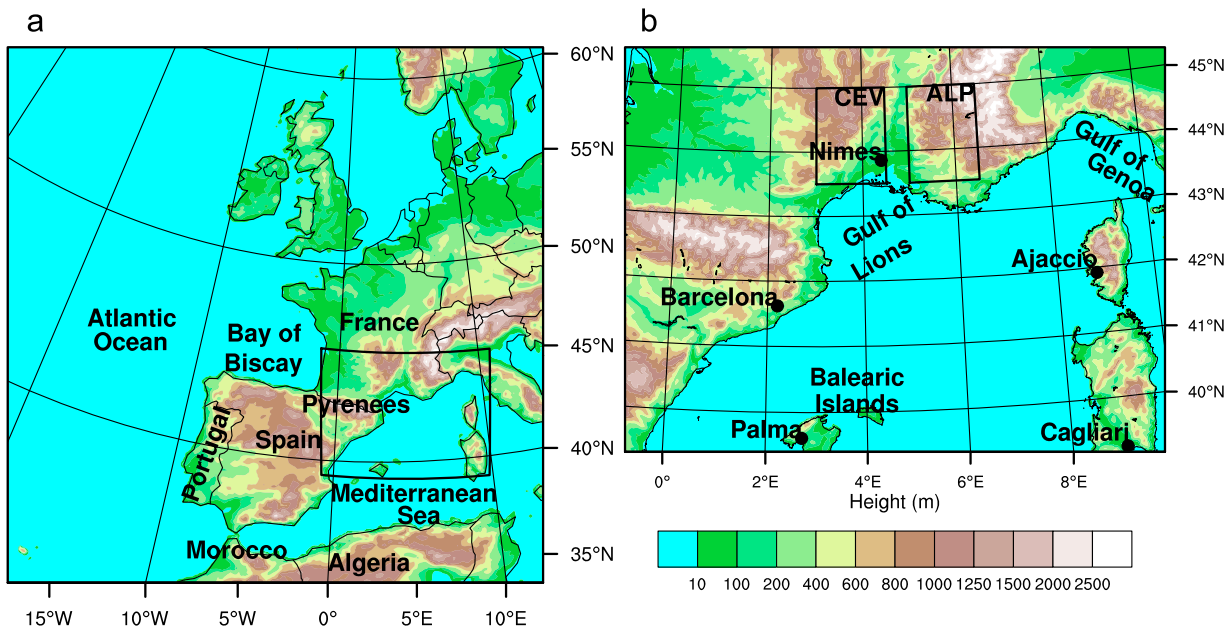


**Figure 1.** Topography (m) of domains used for the Meso-NH experiments: (a) 12 km and (b) 3 km mesh size domains.

the climatological average, the normal monthly accumulated precipitation being 136 and 67 mm at Nimes, and 289 and 244 mm at Mont Aigoual (located in the Cevennes) in October and November, respectively. The event was not as extreme as the 1992 event at Nimes, due in part to the fact that it occurred in late fall when sea surface temperatures over the Gulf of Lions were relatively cold ( $14^{\circ}\text{C}$ ). However, it was unusual in terms of its duration. The multiday duration of the event allows us to follow the development of the situation and compare the performance of the model between convective and nonconvective regimes.

[6] The event was well predicted by the large-scale operational Numerical Weather Prediction (NWP) model ARPEGE (Action de Recherche Petite Echelle Grande Echelle) of Météo-France and a weather warning for the region was issued. However the operational models were unable to predict accurately the amount and location of precipitation within a catchment. The kilometer scale afforded by mesoscale models such as Meso-NH [Lafore *et al.*, 1998] used here or AROME (Application of Research to Operations at Mesoscale), the next-generation Limited-Area Model (LAM) NWP system for Météo-France (operational since December 2008), allows an explicit representation of clouds and precipitation and at the same time, a fine resolution description of the orography of the catchment.

[7] The purpose of the present study is to use satellite observations to assess the ability of a mesoscale model to forecast a heavy precipitation event. Several sets of 24 h Meso-NH simulations were constructed differing in their initial and boundary conditions provided by different operational NWP systems. We evaluated the performance of the Meso-NH model against measurements from a network of rain gauges over France, and to overcome the serious limitation of evaluation over land only, the assessment was extended over the sea through the use of satellite data. Satellite data are potentially extremely useful in monitoring heavy precipi-

tation in the Mediterranean as weather systems arrive from the sea where ground-based observations are sparse. From satellite observations we can identify the location of clouds and precipitation, and thereby assess the ability of the model to predict the correct quantity of precipitation along with the correct reason.

[8] In section 2 we describe the model, the numerical experiments and the evaluation approach. Section 3 contains an overview of the case study at the synoptic scale, and describes the resulting accumulated precipitation over land during this 5 day episode. Section 4 presents the time evolution of the event, and two particular days, 20 and 22 November, which were characterized by stratiform and convective precipitation, respectively. The sensitivity of the precipitation forecast to the initial conditions is then discussed. Section 5 concludes the paper.

## 2. Numerical Experiments and Evaluation Approach

### 2.1. Numerical Experiments

[9] The numerical simulations were performed with the nonhydrostatic mesoscale model Meso-NH [Lafore *et al.*, 1998] version 4.8. The two-way interactive grid-nesting method [Stein *et al.*, 2000] enabled the simultaneous running of several models on the same vertical levels but with different horizontal resolutions. The case was simulated with either doubly nested models or a single model. The vertical grid had 50 levels up to 20 km with the levels spaced from 60 m close to the surface to 600 m at high altitudes. The exterior domain was centered over western Europe with a horizontal grid spacing of 12 km, and a second interior domain was centered over the Cevennes with a 3 km grid spacing. The domains of the simulations are shown in Figure 1.

[10] For the coarser-resolution grid, the subgrid-scale convection was parameterized by a mass flux convection scheme

**Table 1.** Meso-NH Experiments

| Experiments | Number of Models | Grid Spacing | Coupling |
|-------------|------------------|--------------|----------|
| ECM         | 2                | 12 and 3 km  | ECMWF    |
| ARP         | 2                | 12 and 3 km  | ARPEGE   |
| ALA         | 1                | 3 km         | ALADIN   |

[Bechtold *et al.*, 2001], while for the inner grid, explicit deep convection was permitted, switching off the parameterization scheme. The parameterization of turbulence was based on a 1.5-order closure [Cuxart *et al.*, 2000]. The shallow convection was parameterized using an eddy diffusivity mass flux scheme [Pergaud *et al.*, 2009]. The microphysical scheme included the three water phases with five species of precipitating and nonprecipitating liquid and solid water [Pinty and Jabouille, 1998] with a modified ice to snow autoconversion parameterization following Chaboureau and Pinty [2006]. Subgrid-scale cloud cover and condensate content were parameterized as a function of the normalized saturation deficit by taking both turbulent and convective contributions into account [Chaboureau and Bechtold, 2002, 2005]. The surface energy exchanges were represented according to four possible surface types (natural vegetation, urban areas, ocean, lake) included in a grid mesh. The Interactions between Soil, Biosphere and Atmosphere (ISBA) scheme [Noilhan and Planton, 1989] was used for natural land surfaces. The turbulent air-sea fluxes were parameterized following the bulk iterative Exchange Coefficients from Unified Multi-campaigns Estimates (ECUME) scheme [Belamari, 2005]. The radiative scheme was the one used at the European Centre for Medium-Range Weather Forecasts (ECMWF) [Gregory *et al.*, 2000] including the Rapid Radiative Transfer Model (RRTM) parameterization [Mlawer *et al.*, 1997].

[11] Three sets of simulations were performed starting at 0000 UTC each day from 19 to 23 November. Each simulation was repeated using three different sets of initial and boundary conditions, provided either by the operational global assimilation NWP system of ECMWF and ARPEGE (ECM and ARP, respectively), or the operational mesoscale assimilation of ALADIN/France (Aire Limitée Adaptation Dynamique développement InterNational) (experiment ALA). ALADIN is a LAM for which the boundary conditions are provided by the ARPEGE model. These NWP systems use four-dimensional (ECMWF, ARPEGE) or three-dimensional (ALADIN) variational assimilation. ARPEGE and ALADIN share the same physics. The ALADIN/France system differs from the two others in the resolution of the analysis providing short-range forecasts over western Europe with a 10 km horizontal assimilation [Fischer *et al.*, 2005]. For ECM (ARP), the lateral boundary conditions for the outermost domain were updated every 6 h by large-scale ECMWF (ARPEGE) operational analyses. Boundary conditions were provided by the outer model for the inner model at every time step (two-way nesting procedure). For the ALA experiments, the initial/boundary conditions were provided by mesoscale operational analyses/3 h forecasts directly on the inner domain. Thus in this case, Meso-NH was run only on the inner domain as the outer domain is not covered by ALADIN. The different Meso-NH simulations are summarized in Table 1.

## 2.2. Evaluation Approach

[12] For the first part of the evaluation, we compared the amount of precipitation measured by rain gauges over France with the simulated precipitation on a 3-hourly basis. Each rain gauge was compared with the nearest model grid point and precipitation was averaged over the rain gauges situated within the inner domain. To quantify the ability of the model to forecast a precipitation event at the right location, the categorical Equitable Threat Score (ETS) was used. ETS measures the fraction of correct forecasts after eliminating those which would be correct due to chance. Values of ETS are by definition less than 1, 1 being the perfect score. A zero ETS value means that all successful forecasts can be attributed to the chance while negative ETS indicates forecast less good than a random forecast.

[13] The use of rain gauges limited the evaluation to land area only. To complement this, we evaluated simulations against Meteosat Second Generation (MSG) observations using the so-called model-to-satellite approach [Morcrette, 1991]. This approach consists of calculating any remotely sensed radiative quantity from the predicted model fields, allowing a direct comparison with coincident observations from satellite. It offers the advantage that the satellite data are used without being combined with any ancillary data, thus avoiding the possible impact of inconsistent assumptions between simulated and retrieved geophysical fields. The approach was first used in Meso-NH to identify discrepancies in the forecast of cloud cover using infrared observations from geostationary satellites [Chaboureau *et al.*, 2000, 2002].

[14] The model-to-satellite approach is a useful tool for verifying mesoscale forecasts. The MSG observations have a horizontal resolution comparable to that of the model used (3 km at subsatellite point) and are available on a regular temporal scale of 15 min. Here, we used hourly measurements of brightness temperature (BT) at 10.8  $\mu\text{m}$  which is mainly affected by cloud-top heights. These observations were projected onto the inner Meso-NH grid. Synthetic BTs were computed from the model output using version 8.7 of the radiative transfer code developed for the Tiros Operational Vertical Sounder (RTTOV) [Saunders *et al.*, 2005].

[15] In addition to measurements in the infrared, we also used measurements made in the microwave region. Since microwave radiation penetrates clouds, its sensitivity to cloud content, which depends on the frequency, allows us to characterize the convective nature of clouds. The Advanced Microwave Sounding Unit (AMSU-B) offers such an observation about every 6 h and with a near-nadir resolution of 16 km. Following Funatsu *et al.* [2007], we used the observations from AMSU-B moisture channels (3 to 5 centered at 183 GHz) to detect the presence of hydrometeors through the scattering of radiation, which lowered the BT compared with its surroundings. Funatsu *et al.* [2007] showed that the difference between channels 3 and 5 (hereafter, B3m5) of greater than  $-8$  K corresponded statistically to precipitation of at least 10 mm in 3 h when compared to the 3-hourly-accumulated rainfall from Tropical Rainfall Measuring Mission (TRMM) data over the Mediterranean basin. In addition, we used a deep convection threshold (DCT) taken from Hong *et al.* [2005] to detect deep convection over the Mediterranean. DCT was defined such that B3m5, B4m5 and B3m4 (i.e., AMSU-B channels 4 minus 5, and 3 minus 4, respectively) were simultaneously equal to or

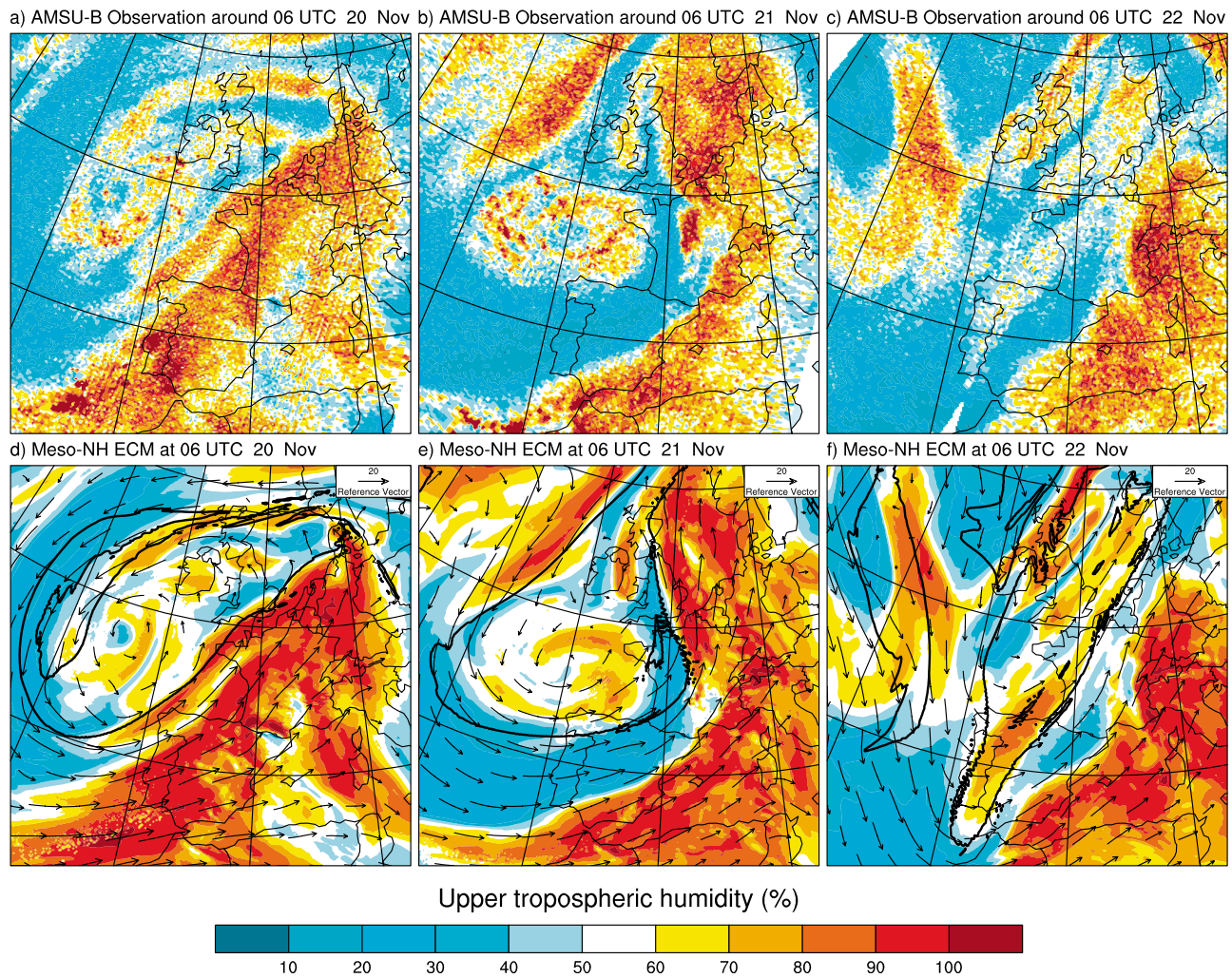


**Figure 2.** Upper-level conditions: UTH (%) from (a, b, c) AMSU-B observation and (d, e, f) Meso-NH ECM simulations at 0600 UTC 20, 21, and 22 November 2007. In Figures 2d, 2e, and 2f the vectors represent the 500 hPa wind ( $\text{m s}^{-1}$ ) and the black line represents the 300 hPa potential vorticity (PV) at 2 PVU ( $\text{PVU} = 10^{-6} \text{ m}^{-2} \text{ s}^{-1} \text{ kg}^{-1}$ ). AMSU-B observations were from NOAA-15 at 0630 UTC and NOAA-16 at 0450 and 0600 UTC 20 November, NOAA-15 at 0540 UTC and NOAA-16 at 0620 UTC 21 November, and NOAA-15 0515 UTC and NOAA-16 at 0610 UTC 22 November.

larger than zero. We also used AMSU-B channel 3 observations which were transformed into upper-tropospheric humidity (UTH) with respect to ice using the formulation proposed by Buehler and John [2005]. This transformation was applied both to the observed and simulated BTs for a direct comparison.

[16] Measurements at lower frequency from the Special Sensor Microwave Imager (SSM/I) on board the Defense Meteorological Satellite Program's (DMSP) F13, F14, and F15 satellites were also employed. From SSM/I, the 37 GHz V and H channels (where V and H stand for vertical and horizontal polarization, respectively) were used to detect rain over sea. Observations were available twice a day, around 0600 and 1800 UTC, and with a resolution of  $37 \text{ km} \times 28 \text{ km}$  and a spatial sampling of 25 km. For frequencies less than or equal to 37 GHz, the emission produced by rain dominates and increases the BT. In particular, when the BT for the 37 GHz V channel is greater than 229 K it is considered as rain [Petty, 1994]. A 37 GHz polarization ( $\Delta 37$ ) of less than 30 K is used to flag pixels as rainy [Goodberlet *et al.*, 1989] while

$\Delta 37$  greater than 40 K is considered as good indicator for the absence of rain over water [Kummerow and Giglio, 1994].

[17] Lastly, the SSM/I observations were used to retrieve the surface wind speed using the algorithm of Goodberlet *et al.* [1989] and the precipitable water (or vertically integrated water vapor content) using the algorithm of Petty [1994]. The retrievals are based on the channels at 19, 22 and 37 GHz. All of them have a spatial sampling of 25 km, but their resolution decreases with decreasing frequency, the lowest resolution being  $69 \text{ km} \times 43 \text{ km}$  for the 19 GHz channels. The AMSU and SSM/I observations were interpolated onto the outer Meso-NH grid.

### 3. Case Study Overview

#### 3.1. Synoptic Situation

[18] We begin by describing the synoptic-scale meteorological situation at upper levels that occurred during the 3 days central to the 5 day period. Figure 2 shows UTH from

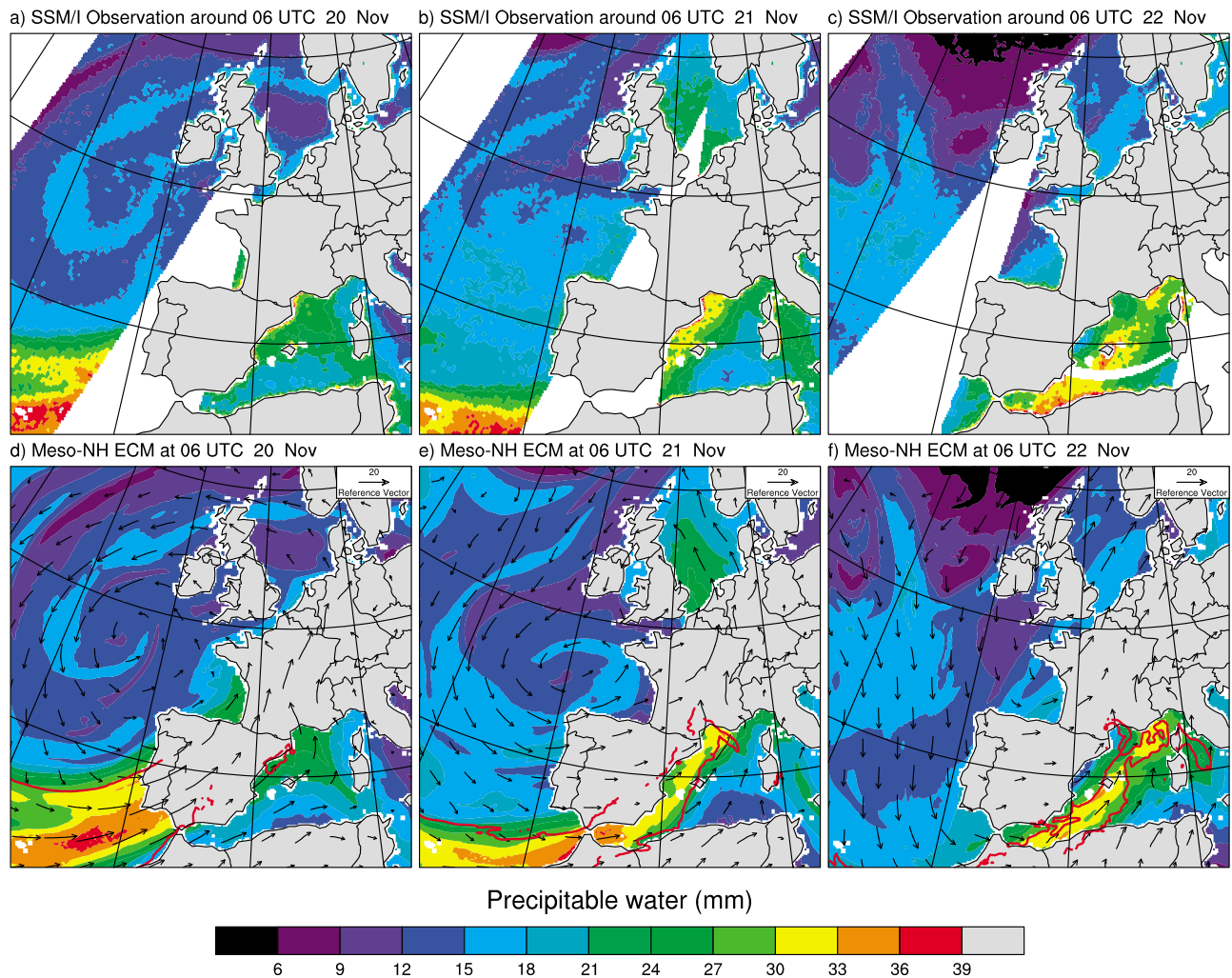


**Figure 3.** Low-level conditions: precipitable water (mm) from (a, b, c) SSM/I observations and (d, e, f) Meso-NH ECM simulations at 0600 UTC 20, 21, and 22 November 2007. In Figures 3d, 3e, and 3f the vectors and the red line represent the 850 hPa wind ( $\text{m s}^{-1}$ ) and the 925 hPa equivalent potential temperature at 315 K, respectively. SSM/I observations were from DMSP-F14 at 0520 and 0700 UTC 20 November, DMSP-F14 at 0505 and 0640 UTC 21 November, and DMSP-F13 at 0700 and 0840 UTC 22 November.

AMSU-B observations and the Meso-NH ECM simulations. Observed and simulated UTH showed similar structures during these 3 days. Quantitative comparison between UTH fields gave a bias around 7%, a standard deviation of 15% (figures are given in terms of absolute values), and a correlation coefficient between 0.76 and 0.80.

[19] On 20 November, both observed and simulated UTH (Figures 2a and 2d) displayed an ellipsoid pattern with a southwest-northeast orientation over the Atlantic ocean. As shown by the 500 hPa wind vectors, the UTH pattern rolls cyclonically within a region of high PV at 300 hPa, indicating a lowering of the dynamical tropopause off the Atlantic coast. This led to a southwesterly flow over western Europe associated with an extensive area of cloud cover as revealed by high values of UTH. Areas where UTH was greater than 100% suggest the occurrence of deep convection off the Moroccan coast, over Portugal and off the southern part of the French Atlantic coast. The Meso-NH ECM simulation reproduced these areas fairly well, but wrongly fore-

casted high-level clouds over the eastern Pyrenees. The absence of high cloud over southeastern France, where the 500 hPa circulation was slightly diffluent, was correctly simulated.

[20] On 21 November (Figures 2b and 2e), the upper-level cyclonic center moved eastward over the Bay of Biscay. Areas where UTH was less than 20% can be seen over Spain suggesting the intrusion of dry stratospheric air in the troposphere. In the observed and simulated fields, high UTH can be seen along the Greenwich Meridian and on the western side of the Mediterranean Sea extending from the Strait of Gibraltar to southeastern France. Areas of  $\text{UTH} > 100\%$  were also evident, with the largest spatial extent over northern France, Benelux, and around the Strait of Gibraltar. Over the Gulf of Lions, UTH was  $< 100\%$  and the 500 hPa wind was no longer diffluent.

[21] On 22 November (Figures 2c and 2f), UTH developed into a more characteristic elongated form along the southwest-northeast axis, indicative of a trough, which is often present

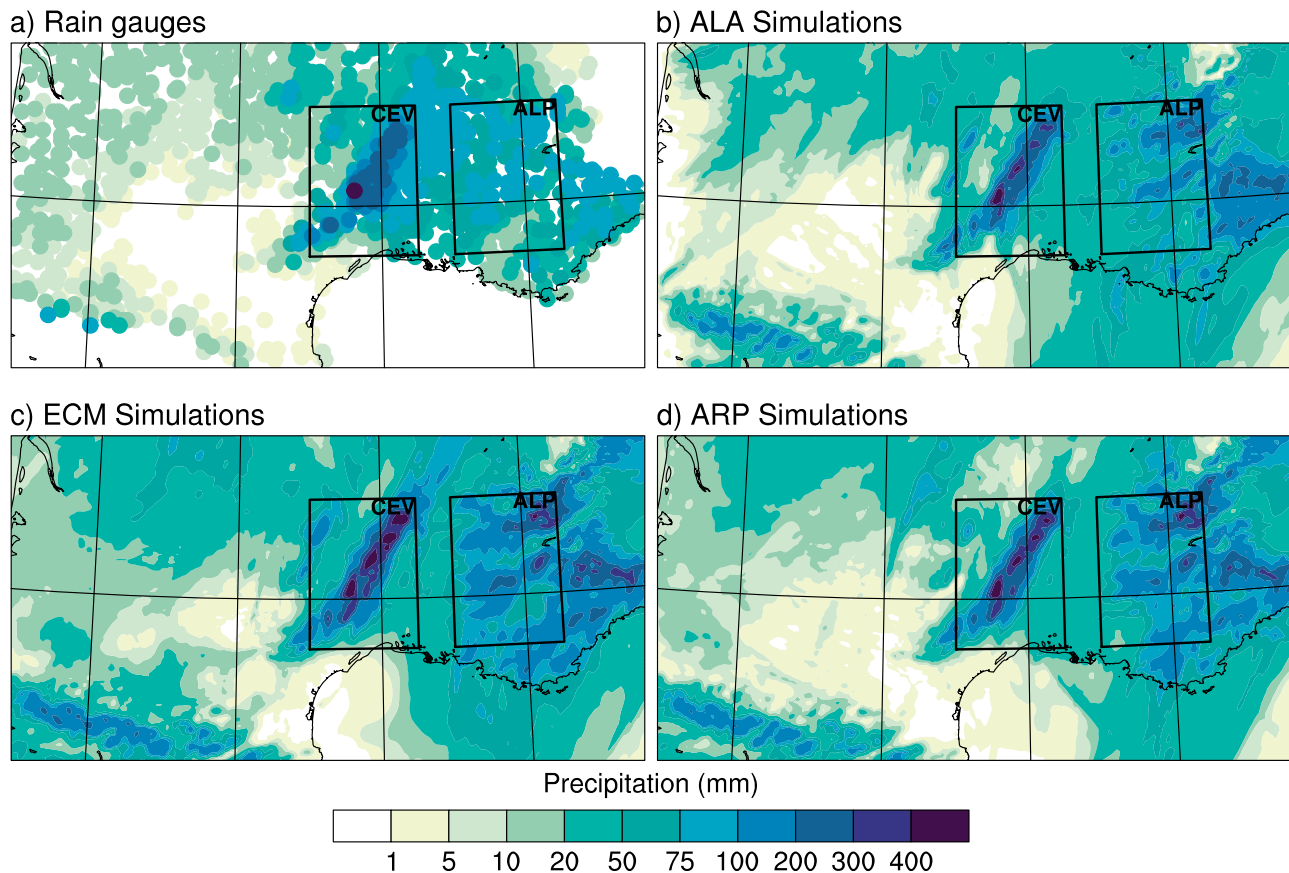


**Figure 4.** Accumulated precipitation (mm) between 0000 UTC 19 November and 0000 UTC 24 November 2007 from (a) rain gauges (over France only) and (b) ALA, (c) ECM, and (d) ARP simulations.

during events of heavy precipitation in the Cevennes [e.g., *Funatsu et al.*, 2009]. The 500 hPa wind remained southwesterly over southern France. Both observed and simulated UTH exceeded 100% over the Alps where a peak in precipitation was recorded (as shown in Figure 6). The following day, the upper-level trough broke up and precipitation ceased in the region of interest.

[22] For the same dates selected in Figure 2, the precipitable water from the SSM/I observations and the Meso-NH ECM simulations are shown in Figure 3. In addition, the wind at 850 hPa and the equivalent potential temperature at 925 hPa are shown with vectors and red lines, respectively. As for the UTH field, the simulated precipitable water presented very similar structures to those observed. Quantitative comparison between precipitable water fields gave a bias ranging between  $-0.4$  mm and  $0.5$  mm, a standard deviation not larger than  $1.6$  mm, and a correlation coefficient around  $0.95$ .

[23] On 20 November, a structure of low values of precipitable water (Figures 3a and 3d) can be seen at about the same position as the UTH cyclonic structure over the Atlantic ocean (Figures 2a and 2d). Southwest of this low-level low, warm, moist air with precipitable water greater than  $30$  mm was advected southwesterly from Morocco toward the Iberian Peninsula and the Pyrenees. The 850 hPa wind fields showed that a stronger southerly flow had developed over the Mediterranean Sea with wind speeds

reaching  $30 \text{ m s}^{-1}$  along with a southwesterly flow from Spain toward the Pyrenees. The precipitable water over the Gulf of Lions remained moderate with values less than  $24$  mm.

[24] On 21 November, as for the upper-level low (Figures 2b and 2e), the low-level cyclonic center (Figures 3b and 3e) moved eastward over the Bay of Biscay. There was a southwesterly flow from the Mediterranean Sea and warm, moist air on the western side of the Mediterranean Sea. As a consequence, the Gulf of Lions experienced a significant increase in precipitable water with values reaching  $30$  mm. Note that the ECM simulation overestimated the precipitable water there by a few millimeters. The 925 hPa equivalent potential temperature was also enhanced in the area.

[25] On 22 November, there was no longer a cyclonic flow over the Bay of Biscay. The warm, moist air spread from the Algerian coast to the Gulf of Genoa passing through the Balearic Islands. The 850 hPa flow was again southwesterly over the western Mediterranean Sea. The values of equivalent potential temperature at 925 hPa were much higher than on previous days. As a result, the values of Convectively Available Potential Energy (CAPE) were increased with respect to 21 November as discussed in section 4. This combined with the southwesterly flow led to convective storms over the sea and a large amount of precipitation over land. Finally, on 23 November, the 850 hPa southwesterly flow over the Mediterranean Sea was weaker and located to the east of the  $5^\circ$  meridian while winds were northerly in the vicinity of

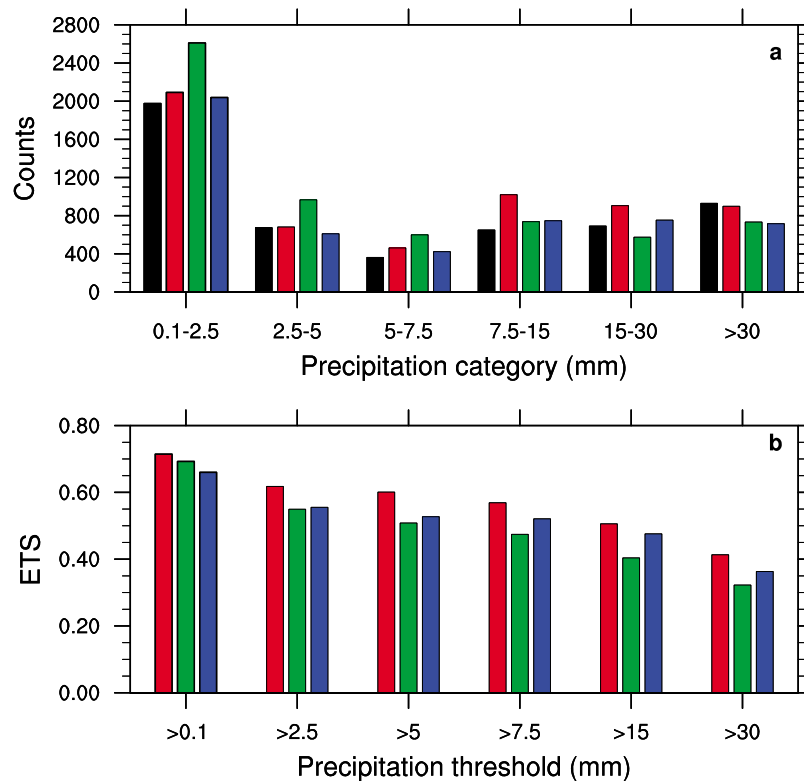


**Figure 5.** (a) Histogram for the 24 h accumulated precipitation of rain gauges and Meso-NH simulations. (b) ETS score for the 24 h accumulated precipitation. Results are from all the Meso-NH simulations performed starting from 19 to 24 November 2007. Code color is black for observation, red for ECM, green for ARP, and blue for ALA.

the Cevennes. Precipitation was thus confined to a small area of southeastern France (not shown) and the weather warning was lifted by 0700 UTC.

[26] From Figures 2 and 3 it appears that the ECM simulations reproduced the structures of moisture at upper and lower levels fairly well. Similar results were obtained with the ARP simulations (not shown). In section 4, we see that these simulations were fairly successful in forecasting the 24 h accumulated precipitation over southern France but failed to predict precipitation accurately at the local scale.

### 3.2. Accumulated Precipitation Over Land

[27] Figure 4 shows the modeled and recorded precipitation accumulated over the 5 day episode. The statistics were based on 1700 rain gauges each day. The quantities of precipitation accumulated over the 5 days were quite realistic, and the precipitation was well localized for all the simulations with two areas being particularly dominant. The heaviest precipitation was recorded in the CEV subdomain, defined as 43.5°N–45°N; 3°E–4.5°E and covering an area of 1200 km<sup>2</sup> (see also Figure 1b). A maximum of 426 mm was measured while 588, 590, and 556 mm were simulated by ECM, ARP, and ALA, respectively. A second area of heavy precipitation was associated with the Alps (ALP: 43.5°N–45°N; 5°E–6.5°E, also 1200 km<sup>2</sup>, Figure 1b) where a maximum of 181 mm was measured while 437, 474, and 336 mm were simulated by ECM, ARP, and ALA, respectively. For both regions, the maximum values were overestimated with ALA being closest to the observations. In the

Rhone valley, lying between these two subdomains, the observed precipitation was greater than 100 mm and was under predicted by all the simulations (forecast precipitation was between 50 and 75 mm). This illustrates the orographic nature of the precipitation and the importance of orographic forcing in the model that enhanced its capability to predict precipitation at the right location.

[28] A histogram (Figure 5a) shows for each simulation, the distribution of modeled and observed precipitation accumulated over each 24 h period across the rain gauge sites situated within the inner domain. The histogram is independent of location so only the number of sites where a given quantity of precipitation was recorded after 24 h, are counted. The simulations reproduced this distribution well. ARP slightly overestimated the two categories of less than 5 mm of precipitation, but there is no outstanding difference in the 24 h accumulated precipitation between the simulations.

[29] The ability of the model to forecast precipitation over a certain threshold and at the right location was quantified with the ETS (Figure 5b). It was calculated for the 24 h accumulated precipitation during the 5 day episode over the inner domain. The ETS for the >0.1 mm category is rather high, around 0.7, in all the simulations. This was expected due to the importance of the orographic forcing in this event. For the other categories, the ETS decreased as the threshold increased. This was also as expected since heavy precipitation events are less frequent in time and space [e.g., Richard *et al.*, 2007]. A higher ETS was found for ECM whatever the precipitation category while ALA performed

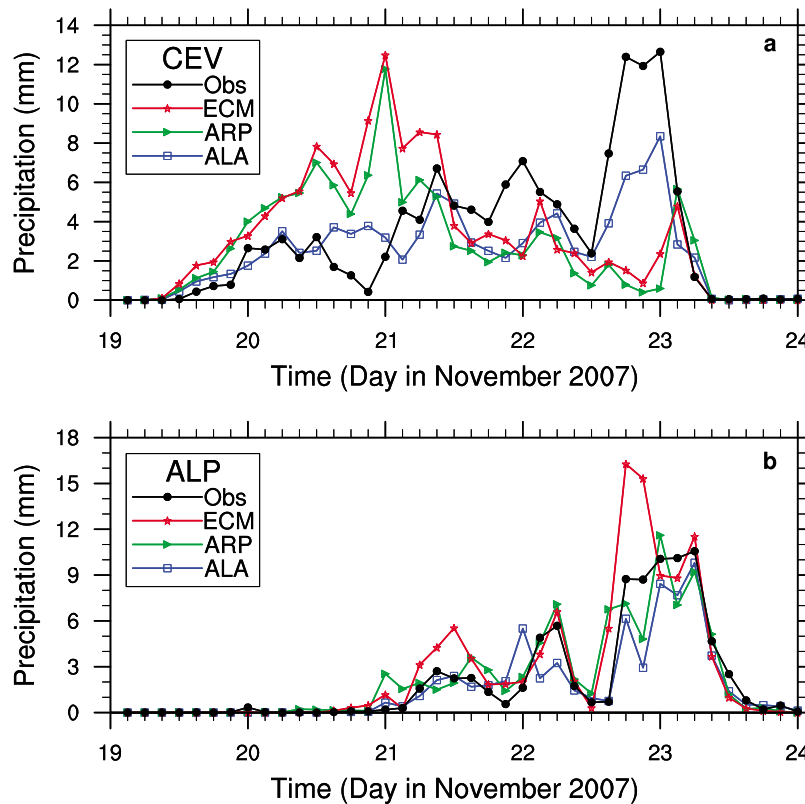


**Figure 6.** Time series of 3 h accumulated precipitation (mm) averaged over the (a) CEV and (b) ALP subdomains. Outputs from each 24 h simulation are every 3 h from  $t + 3$  to  $t + 24$ .

better than ARP in general. These results suggest that the model succeeded well in simulating the 24 h accumulated precipitation during this 5 day episode. We can conclude therefore, that the difference in initial conditions did not significantly affect the forecast of 24 h accumulated precipitation.

[30] A very different picture is obtained from the time series of 3-hourly precipitation averaged over the CEV and ALP subdomains (Figure 6). The forecasting skill changes dramatically with the location of precipitation and the set of simulations. This is a key point for all hydrometeorological applications. Indeed, the quality of any flood prediction that is based upon hydrological simulations depends to a high degree upon the quality of the measurements and forecasts of precipitation which are often at a much higher frequency than the 3 h shown here.

[31] Over the CEV subdomain (Figure 6a), there was almost continuous precipitation from 19 to 23 November with the greatest intensity in the afternoon of 22 November. The forecasted intensity of precipitation presents some disagreements. Moderate precipitation (such as on 19–21 November, and particularly 20 November) was overestimated by ECM and ARP but the heavy precipitation on 22 November was remarkably underestimated. The intensity of the precipitation as forecast by ALA agreed much better with the observations. This can be ascribed to the different configuration of the model Meso-NH, including different initial and boundary conditions provided by ALADIN.

[32] Over the ALP subdomain (Figure 6b), precipitation occurred between 21 and 23 November with the heaviest

amount during the morning of 23 November. Again, the simulations performed well in capturing the occurrence of this episode of precipitation, displaying a better agreement with the observations than for the CEV subdomain. An exception to this, was the overestimation of precipitation by ECM in the afternoon of 22 November, when it was underestimated by ARP and ALA by a factor of 2. In section 4, we detail the time evolution of the event and use satellite observations to explain the observed discrepancies in the precipitation forecast observed at the 3 h time scale. In particular, the satellite observations highlight the poor prediction of some convective systems that developed over the sea.

## 4. Subsynoptic Features

### 4.1. Radiosonde Measurements

[33] The simulations were first evaluated against radiosoundings taken from the meteorological stations Palma, Barcelona, Nimes, Ajaccio, and Cagliari which lie within the inner domain (see locations in Figure 1). Note that there were no measurements for some stations and dates, for example at 1200 UTC 20 November and 0000 UTC 21 November at Nimes. A quantitative evaluation was made for two fields, precipitable water and CAPE, that integrate atmospheric information from the vertical. CAPE is a measure of convective instability that gives an indication of the possibility of convective storms. It is defined as the vertical integral of the lifted-parcel buoyancy from the level of free convection to the level of neutral buoyancy. The value of CAPE depends on the departure level from which the air parcel is lifted. For

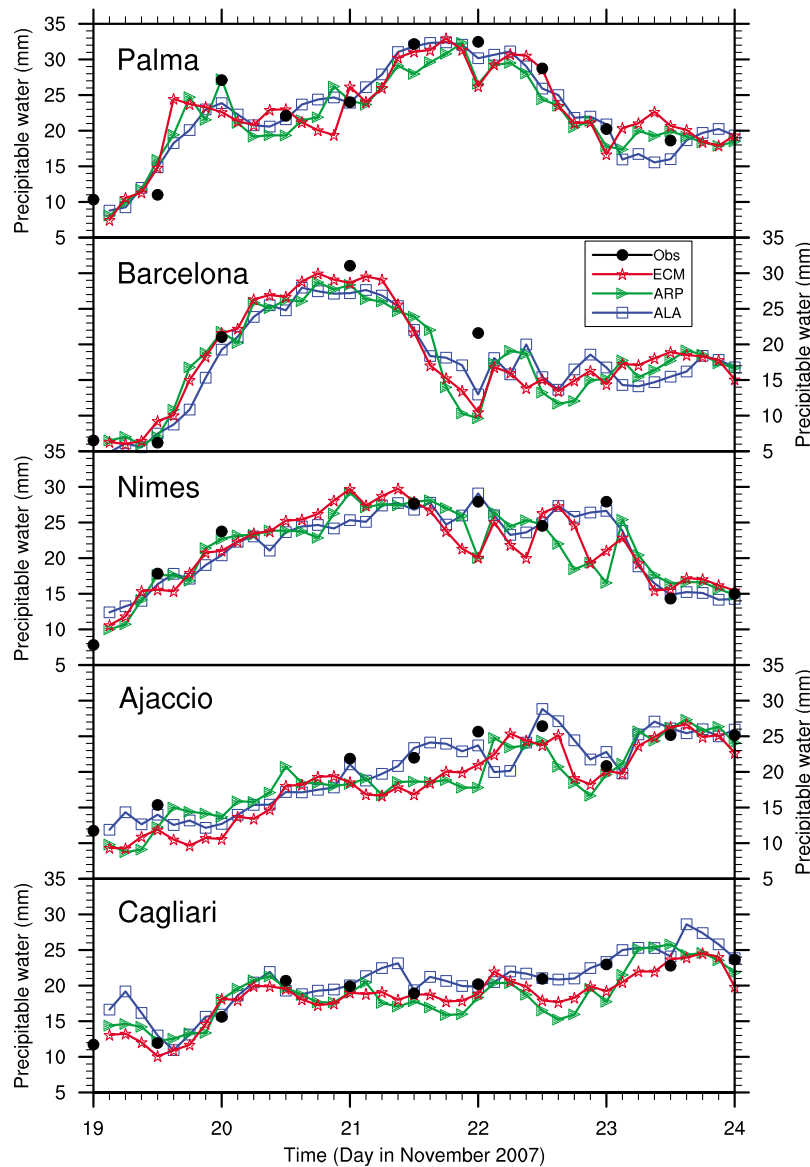


**Figure 7.** Precipitable water (mm) from radiosondes and Meso-NH simulations at five western Mediterranean stations: Palma, Barcelona, Nimes, Ajaccio, and Cagliari. Outputs from each 24 h simulation are every 3 h from  $t + 3$  to  $t + 24$ .

the simulations, the computations of CAPE were performed for each model level and we used the maximum value obtained. For the observations, we used the CAPE given with the radiosonde measurements delivered by the University of Wyoming.

[34] As seen in the synoptic-scale fields (Figure 3), precipitable water at the five stations changed significantly during the episode (Figure 7). A large increase from 5–10 mm to 25 mm occurred during the afternoon of 19 November at those stations on the northwestern side of the Mediterranean sea, i.e., Palma, Barcelona, and Nimes. At Barcelona, the precipitable water increased to a maximum of 31 mm late on 20 November, then decreased to 15–20 mm on 21 November. At Palma, the precipitable water peaked a day later (32 mm on 22 November) and decreased thereafter, and at Nimes, in the foothills of the Cevennes, precipitable water

increased by about 25 mm from 20 to 23 November. In contrast, at the eastern stations, Ajaccio and Cagliari, there was a gradual increase in precipitable water during the 5 day period along with the eastward propagation of the warm, moist air shown in Figure 3.

[35] This large-scale evolution of precipitable water was well captured by the model. This is expected as the model was restarted at 0000 UTC each day from the analyses. The largest departure from observations was usually seen at 0000 UTC each day as we compared model outputs at  $t + 24$ . A better match was obtained for ALA due to the lateral coupling at the boundaries of the inner model. This was particularly true for Palma, Ajaccio and Cagliari located close to the boundaries where the low-level flow entered the domain. At Nimes, the precipitable water showed significant differences between ALA and the two other simulations.

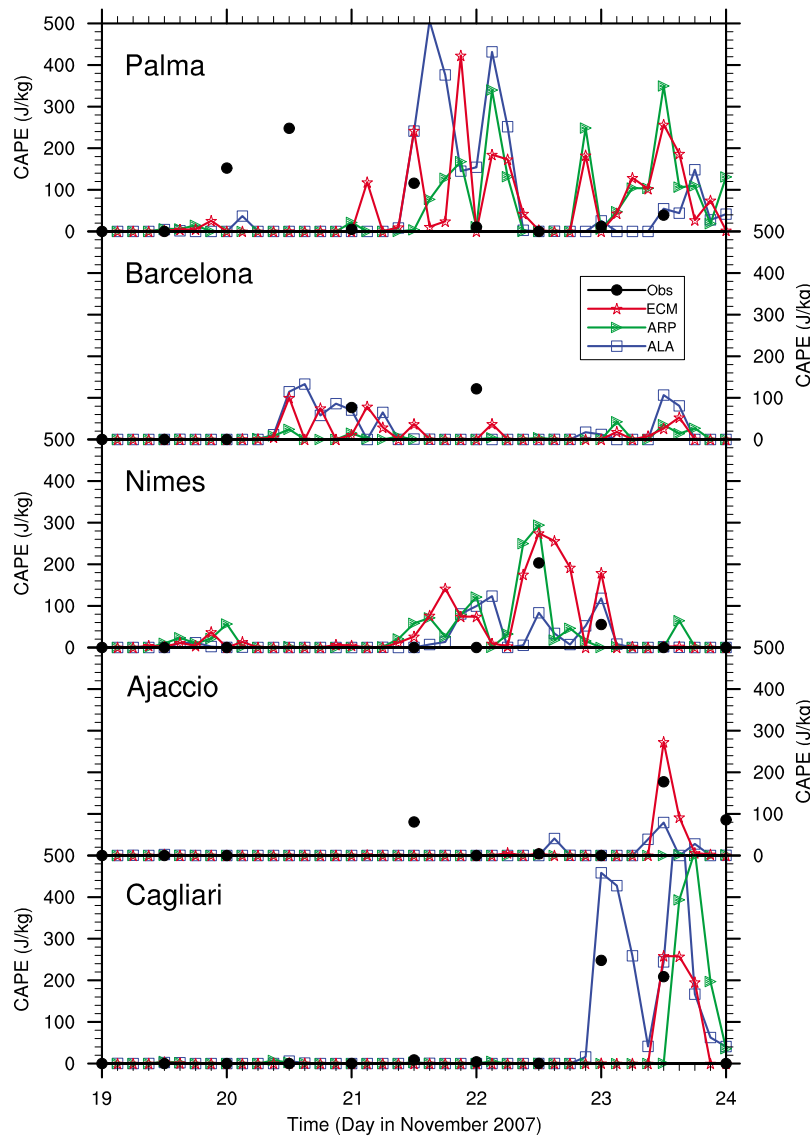


**Figure 8.** Same as in Figure 7 but for CAPE ( $\text{J kg}^{-1}$ ).

With more (less) precipitable water on 20 November afternoon (22 November afternoon), ECM and ARP resulted in more (less) precipitation over the Cevennes than ALA as seen in Figure 6.

[36] CAPE showed an eastward evolution over the 5 days, being zero at all five stations on 19 November and having moderate ( $<300 \text{ J kg}^{-1}$ ) values at Palma on 20 November and at Ajaccio and Cagliari on 23 November (Figure 8). Such values were moderate in comparison with the Cevenole event of 13 and 14 October 1995 [Ducrocq *et al.*, 2008] when CAPE exceeded  $1400 \text{ J kg}^{-1}$ , or 9 September 2002 [Delrieu *et al.*, 2005] when  $850 \text{ J kg}^{-1}$  was recorded at Nimes. The simulations likewise showed this eastward transition, but missed some instances of positive CAPE, for example, at Palma on 20 November and at Ajaccio on 21 November. The simulated values of CAPE were sometimes significantly larger than observed, for example, at Palma on 21 November with values up to  $500 \text{ J kg}^{-1}$ . This contrasts with the agreement obtained for the precipitable water, a field smoother

than CAPE. The poor agreement suggests a limit in the quantitative comparison of CAPE and/or the difficulty in forecasting convective conditions with accuracy.

#### 4.2. Satellite Observations

[37] While the radiosonde data give a good indication of the evolution of the event in the vicinity of the station, a broader picture can be obtained from satellite observations which give a much better coverage over the sea.

[38] The AMSU-B moisture channels give information on the presence of moderate to convective rain over both the sea and the land (Figures 9a–9c). As shown by Funatsu *et al.* [2007],  $B3m5 > -8 \text{ K}$  is an indicator of the occurrence of rain, of at least 10 mm in 3 h, which allows for the detection of moderate rain in the Mediterranean. Small areas of light rain can be seen near the Balearic Islands on 20 November, over northern Spain and western France on 21 November, and several areas of intense rain on 22 November. Over the Cevennes,  $B3m5$  was less than  $-8 \text{ K}$  on 20 and 21 November

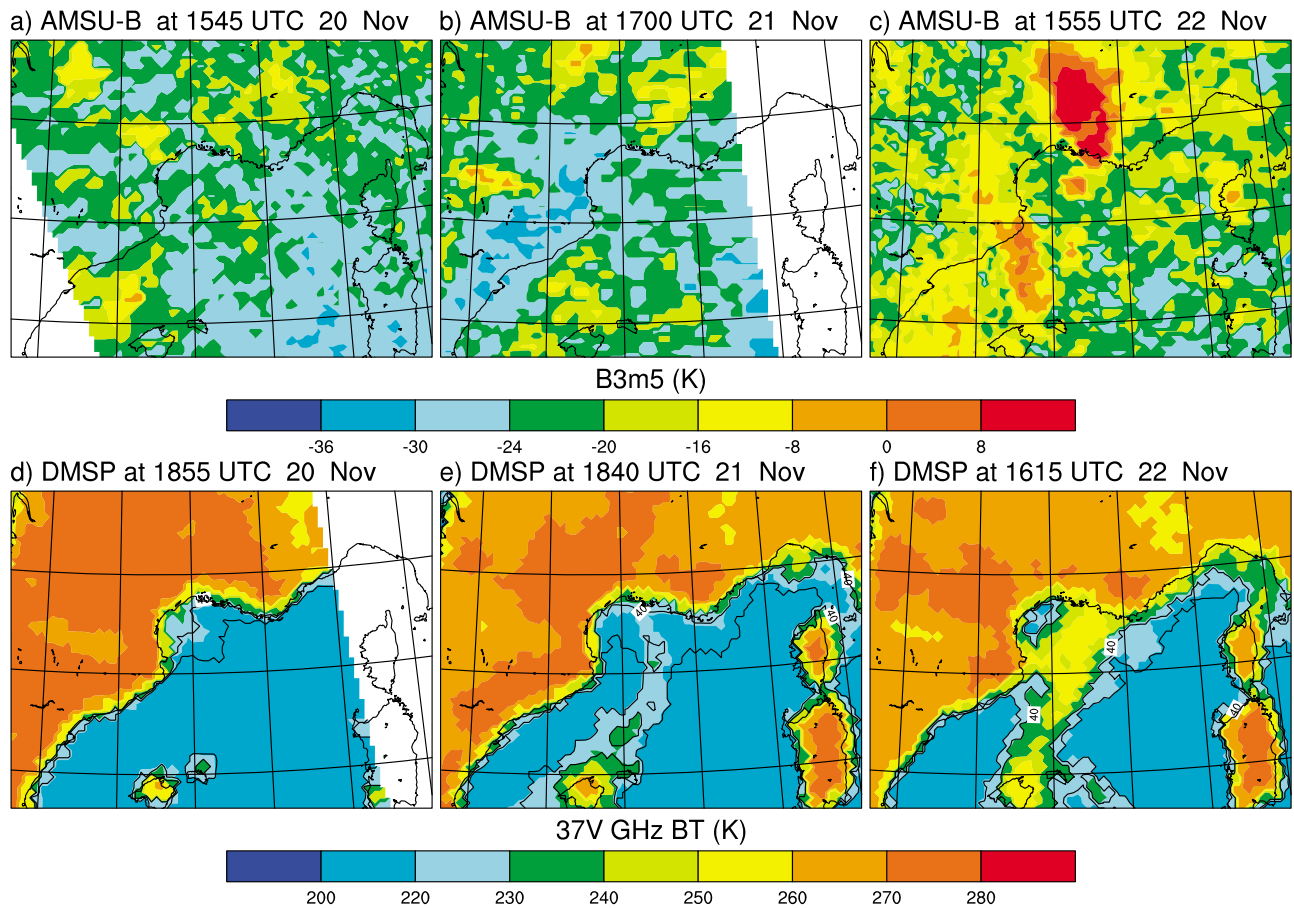


**Figure 9.** Rainy conditions: (a, b, c) B3m5 (K) and (d, e, f) 37V GHz BT (K) from AMSU-B and SSM/I observations, respectively, around 1800 UTC 20, 21, and 22 November 2007. Black line is  $\Delta 37$  at 40 and 50 K. B3m5 were from NOAA-15 at 1545 UTC 20 November, NOAA-15 at 1700 UTC 21 November, and NOAA-16 1555 UTC 22 November. SSM/I observations were from DMSF-F15 at 1855 UTC 20 November, DMSF-F15 at 1840 UTC 21 November, and DMSF-F14 1615 UTC 22 November.

consistent with the small amount of rain recorded there (see Figure 6a). Precipitation on 22 November was more convective in nature, B3m5 was greater than zero over a wide area and the DCT criterion was also attained at 1200 and 1800 UTC. At 1800 UTC there was a corresponding peak in precipitation over the CEV and ALP subdomains seen in Figure 6 and the arrival of an area of low BTs can be seen by MSG on the French Mediterranean coast (Figure 14 discussed later).

[39] This picture is confirmed by observations from the 37 GHz V channel on SSM/I (Figures 9d–9f). No rain was observed over the sea on 20 November, but  $\Delta 37$  was less than 50 K over the Gulf of Lions, indicating the occurrence of low-level clouds. On 21 November, the  $\Delta 37$  level at 50 K delineates a band of cloud between the Balearic Islands and the southern French coast, and the presence of rain over the sea was limited to the vicinity of the Balearic Islands. On 22 November, the arrival of warm, moist air as seen in Figure 3c, led to the formation of a wide area of cloud and precipitation over the sea. The 37V-GHz BT over land decreased during the episode, consistent with the B3m5 observations.

[40] Satellite observations also allow us to monitor several fields of the atmospheric water cycle and the wind speed at the surface during the 5 day period. Averaged observed and

simulated values, calculated for the inner domain every 3 h, are shown for  $10.8 \mu\text{m}$  BT, B3m5  $> -8$  K, 37V GHz BT over the sea only, precipitable water, and wind speed at the surface (Figure 10). Two minima in  $10.8 \mu\text{m}$  BTs are apparent in Figure 10a. On 22 November, the peak in precipitation over France (Figure 10d) corresponds with a minimum in BT and with peaks in B3m5  $> -8$  K, 37V GHz BT and precipitable water over the sea. Some differences among these quantities are noteworthy in explaining the differences in observed and simulated precipitation. On 20 November, ECM and ARP overestimated the surface wind speed over the sea by  $2 \text{ m s}^{-1}$  which may have contributed to the overestimation in the amount of precipitation. On 22 November,  $10.8 \mu\text{m}$  BT was better for all simulations. The ALA simulation of 37V GHz BT was closest to the observations and likewise ALA offered a better prediction of the precipitation. ALA also showed the largest water vapor content in agreement with the peak in precipitation.

[41] To summarize the quality of the simulations for the 5 days, we used the ETS categorial score calculated for the 3-hourly accumulated precipitation and  $10.8 \mu\text{m}$  BT (Figure 11). A threshold of 0.1 mm was chosen for verifying the correct quantity of precipitation and a value of 260 K, corresponding to high-level and midlevel clouds [e.g.,

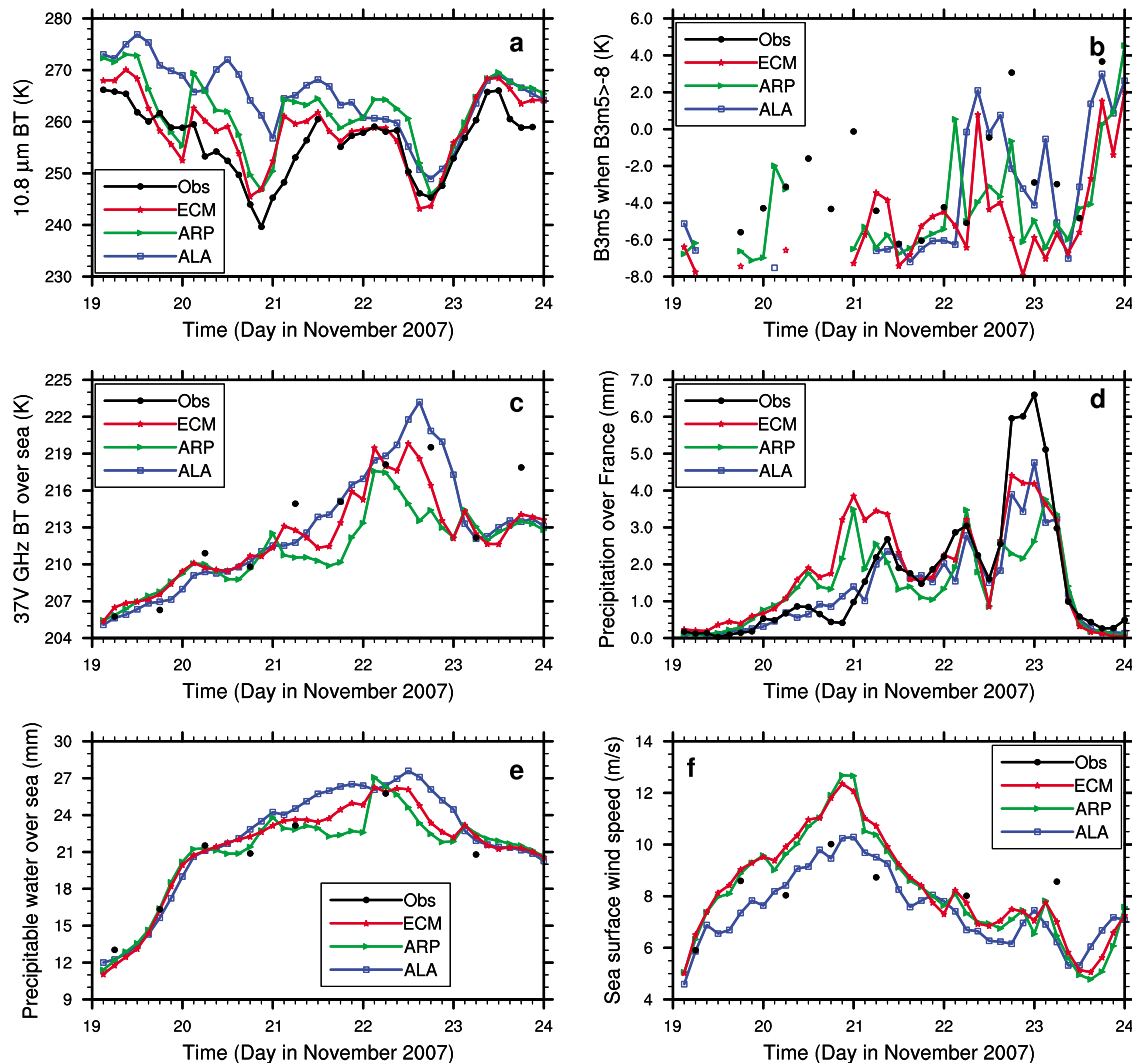


**Figure 10.** Time series of (a)  $10.8 \mu\text{m}$  BT (K), (b) B3m5 (K) when B3m5 is larger than  $-8$  K, (c) 37V GHz BT (K), (d) 3 h accumulated precipitation ( $\text{mm h}^{-1}$ ), (e) precipitable water over sea (mm), and (f) sea surface wind speed ( $\text{m s}^{-1}$ ). Averages were calculated over the inner model domain for  $10.8 \mu\text{m}$  BT and B3m5, over the sea part of the inner model domain for 37V GHz BT, precipitable water, and surface wind speed, and over rain gauges within the inner model domain for the 3 h accumulated precipitation. Outputs from each 24 h simulation are every 3 h from  $t + 3$  to  $t + 24$ .

Chaboureau *et al.*, 2008], was selected to verify the correct location of precipitation. The ETS for precipitation was around 0.3–0.4 indicating that all the simulations performed equally at predicting the occurrence of precipitation (see Figure 10d). However, ALA performed better on the afternoon of 22 November during the convective event over the Cevennes. For the  $10.8 \mu\text{m}$  BT (Figure 11b), high scores were obtained for the overcast conditions in the afternoons of 20 and 22 November. The three simulations showed similar scores except in the afternoon of 20 November. At that time, ECM and ARP were closer to the observed BTs due to a cloud system that developed over the Pyrenees (see also time series of the averaged BTs, Figure 10a). As the cloud system did not produce any significant amount of precipitation, ALA gave the best prediction.

[42] In general, results were better for ALA than ECM and ARP (with the exception of the cloud cover). This was par-

ticularly true for the two days when the forecasts predicted very different amounts of precipitation, thus resulting in different scores. We discuss the reasons for the notable overestimation of precipitation on 20 November and underestimation of precipitation on 22 November in the sections 4.3 and 4.4.

### 4.3. Stratiform Precipitation on 20 November

[43] On 20 November, all three simulations predicted the location of precipitation over the Cevennes, but ECM and ARP forecast almost double the amount of accumulated precipitation than registered by the rain gauges (Figure 10d). A much better result was obtained for ALA. In the afternoon, rainfall eased off according to the observations but continued to increase in ECM and ARP, while remaining almost constant in ALA.

[44] As discussed previously, CAPE indicated a non-convective environment and consistent with this, convective

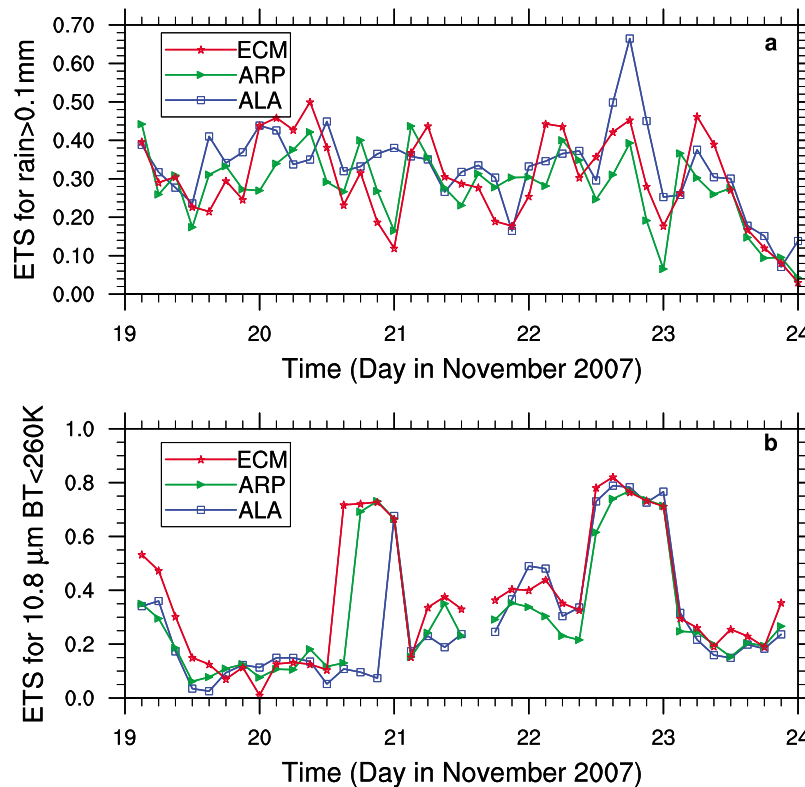


**Figure 11.** Time series of ETS for (a) 3 h accumulated precipitation greater than 0.1 mm and (b)  $10.8 \mu\text{m BT}$  less than 250 K computed over the inner model domain. Outputs from each 24 h simulation are every 3 h from  $t + 3$  to  $t + 24$ .

clouds were absent over the Cevennes (Figure 9a). The low-level southerly flow was strong over the Mediterranean Sea, partly because the Pyrenees deviated the low-level winds along the coast (according to ECM; see the contrast in wind direction between Figures 2d and 3d). The surface wind speed was overestimated by  $2 \text{ m s}^{-1}$  by the ECM and ARP simulations throughout the day while ALA gave a correct averaged wind speed (Figure 10f). To examine the location of this discrepancy and to discuss its impact on precipitation, the surface wind speed for SSM/I observation and the simulations is shown when it was observed at its maximum (1900 UTC 20 November; Figure 12). In addition,  $\Delta 37$  was plotted for the thresholds of 40 and 50 K that were employed for detecting nonprecipitating clouds and absence of clouds, respectively.

[45] The wind speed from SSM/I observations was largest over the Gulf of Lions, where it exceeded  $16 \text{ m s}^{-1}$ .  $\Delta 37$  reached values between 40 and 50 K suggesting the presence of low clouds. In the central part of the domain, the wind was lighter, around  $10 \text{ m s}^{-1}$ , and it was even lighter along the Spanish coast. Simulations agreed with each other in wind direction indicating that the Gulf of Lions was a region of convergence. They all correctly simulated  $\Delta 37$  values less than 50 K, thus the occurrence of low clouds in the right location, but the winds differed greatly in magnitude. In the central part of the domain, ECM and ARP overestimated the wind speed by  $2\text{--}4 \text{ m s}^{-1}$  with respect to the SSM/I retrievals. High wind speeds were also wrongly forecasted along the Spanish coast. In contrast, ALA gave a much better forecast of wind speed.

[46] This was of particular importance to the forecast of precipitation. The low-level wind ensured a continual supply of moisture to the Cevennes throughout the day as witnessed by the gradual increase in the maximum value for the simulated precipitation (Figure 6a) accumulated every 3 h. With the aid of Figure 13, which shows a vertical section taken along the direction of the surface wind over the Cevennes, we can see that this humid layer was lifted orographically and resulted in the large amount of precipitation over the Cevennes. In Figure 13, clouds and precipitating hydrometeors are indicated by the solid black and blue contours, respectively. There was a strong boundary layer flow  $>30 \text{ m s}^{-1}$  for ECM and ARP which overestimated the precipitation.

[47] Some differences among the simulations were also apparent in the free troposphere (Figure 13). ALA shows the lowest cloudiness with precipitation located only over the foothills of the Cevennes. The upper-level jet associated with the trough (see Figure 2d for a general synoptic view) shows a branch at  $42^\circ\text{N}$ . In a moist, windy midtroposphere the ARP simulation showed slightly more developed cloud over land. The position of the upper-level jet is about the same seen in ALA. The precipitation in ALA and ARP was largely stratiform as suggested by the limited vertical development of clouds, and this stratiform precipitation continued throughout the day. In contrast, ECM places the upper-level jet present above the Cevennes at a lower altitude, which induces a destabilization of the atmosphere. The free troposphere was cloudy almost everywhere with precipitating hydrometeors found over land up to 8 km altitude. In consequence, the precipitation was wrongly simulated in front of,

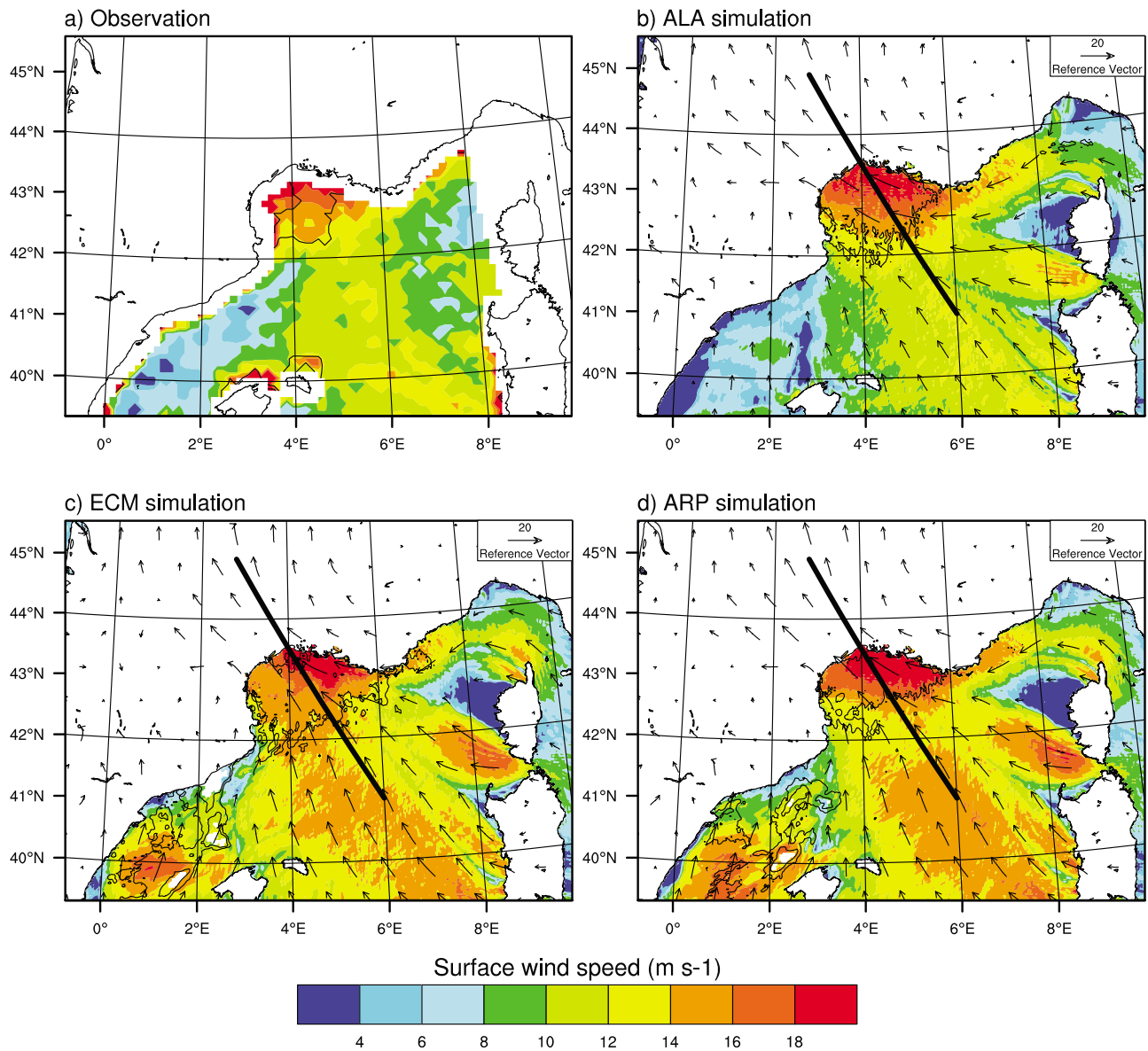


**Figure 12.** Surface wind speed ( $\text{m s}^{-1}$ ) at 1900 UTC 20 November 2007 from (a) SSM/I observation and (b, c, d) Meso-NH simulations (with the wind vector added). Black line is  $\Delta 37$  at 40 and 50 K.

and beyond, the foothills and with quantities which were too large. Unfortunately the lack of radiosoundings for Nîmes at this time did not allow a more quantitative evaluation of the errors in the wind forecast. However we can conclude that the stronger the surface wind, the larger the amounts of precipitation over the Cevennes.

#### 4.4. Convective Regime on 22 November

[48] On 22 November, the precipitation was at its heaviest and led to local flash floods. This was the day characterized by the most intense convective activity. Forecasting these conditions seems to be difficult for models. Indeed, all the models underestimated the amount of precipitation across the inner domain (Figure 10d). The 3 h accumulated precipitation was underestimated by ARP in the afternoon while ECM

forecasted precipitation over the Alps instead of the Cevennes (Figure 6). The best forecast was given by ALA.

[49] We followed the life cycle of convection over the Mediterranean Sea using observations from the satellite MSG. The performance of the model was first investigated on an hourly basis through comparison with MSG. Images of  $10.8 \mu\text{m}$  BT, show clouds which may produce the observed precipitation. In the tropics, low BTs indicate the high convective cloud tops which are quite well correlated with precipitation [e.g., Söhne *et al.*, 2008], although this may evaporate before reaching the ground. At midlatitudes, this correlation is less robust, and here we used a threshold of 225 K as it yielded the correct difference between observation and simulations. Figure 14 shows the times when BTs less than 225 K were observed on 22 November. Although the signature of early BT < 225 K is overlapped by later

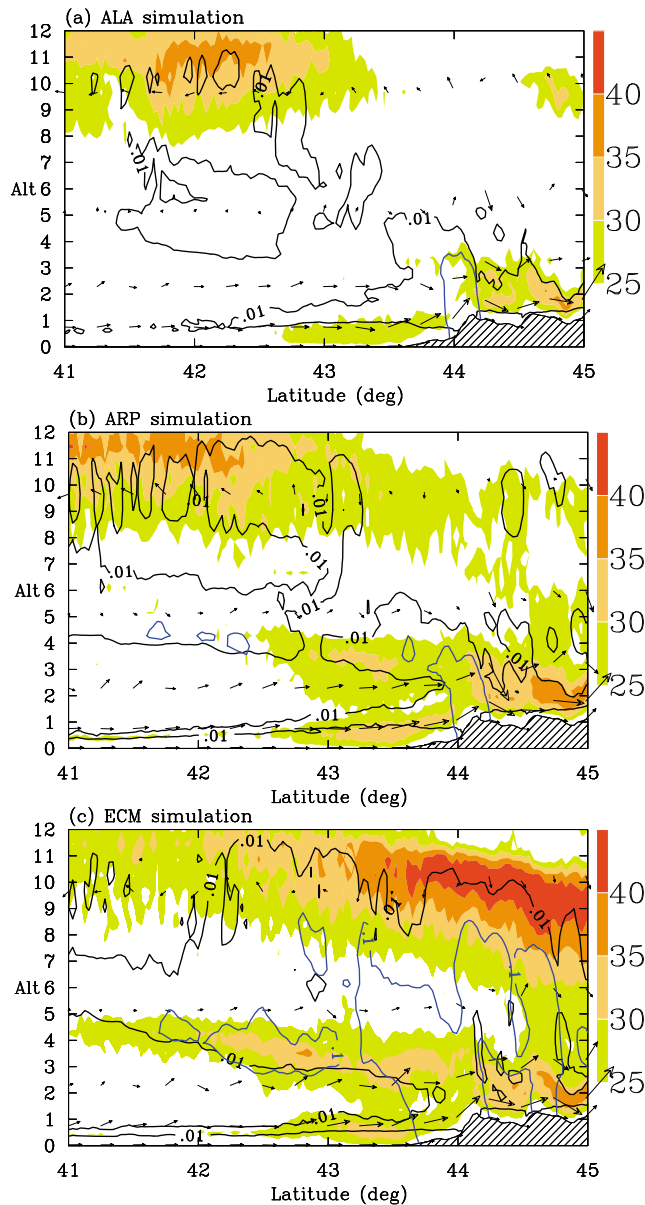


**Figure 13.** Vertical section of wind speed  $>18 \text{ m s}^{-1}$  at 1900 UTC 20 November along the axis shown in Figure 12. Clouds are indicated by the solid black contour showing where mixing ratios for cloud plus ice is greater than  $0.01 \text{ g kg}^{-1}$ . Precipitating hydrometeors are shown by the solid blue contour for the mixing ratios larger than  $0.1 \text{ g kg}^{-1}$ . Results are shown for (a) ALA, (b) ARP, and (c) ECM simulations.

systems, two lines of BT  $< 225 \text{ K}$  starting from the north of the Balearic Islands can be clearly distinguished.

[50] The westernmost line of BT  $< 225 \text{ K}$  appeared at 1100 UTC around  $42^\circ\text{N}$ ,  $3^\circ\text{E}$  in a region where CAPE was positive according to ALA (not shown) but zero according to ARP and ECM. The region of positive CAPE moved toward the French coast resulting in a thunderstorm observed at 1400 UTC over the Cevennes and a consequent first peak in precipitation (Figure 6a). This thunderstorm was triggered by a former one that developed from the Balearic Islands at 0800 UTC ( $41^\circ\text{N}$ ,  $4^\circ\text{E}$ ). The development of thunderstorms over the sea (where observations are sparse) makes the

quantitative precipitation forecast over the Cevennes very challenging. ALA forecasted this line of low BT rather well, but the convective system that reached the Cevennes at 1400 UTC developed a few tens of kilometers too far west, was 1 h later, and was less developed in term of cloud cover. This was however the system that produced the heavy precipitation in the Cevennes and importantly, was missed by ECM and ARP.

[51] The easternmost line of BT  $< 225 \text{ K}$  started at 1600 UTC to the northeast of the Balearic Islands. This line together with the numerous systems born over the Gulf of Lions in the evening resulted in precipitation mostly over the Alps. Apart from the convective system that developed in the morning, the correct evolution of the BT signature was only forecasted by ARP, consistent with a fair prediction of precipitation in the ALP subdomain (Figure 6b). ECM provides a fairly realistic scenario with a phase of convection that began over sea at about the right time and location. The intensification of the storm was however too rapid (convection was triggered at 0400 UTC compared with 0900 UTC in the MSG observation) and the precipitation was overestimated (e.g., 15 mm accumulated in 3 h at 2100 UTC compared with 8 mm observed, Figure 6b). Lastly, ALA gave a realistic prediction of precipitation over the ALP subdomain, but with cloud activity to the east of  $6^\circ\text{E}$  that was too intense.

[52] In the absence of large-scale forcing, it is generally very difficult to predict convection accurately. The initial conditions are of crucial importance for a valuable short-term forecast of convective systems, especially concerning the representation of fine-scale details in the initial humidity fields [e.g., *Ducrocq et al.*, 2002]. The only observation relevant to the triggering of the convection available over the sea is the precipitable water. The precipitable water is shown at 0700 UTC, the closest time to the first SSM/I observation after the start of the model (Figure 15). The simulated CAPE was also shown at the values of 200 and  $400 \text{ J kg}^{-1}$ .

[53] A strip where values of precipitable water were greater than 27 mm extended from the Balearic Islands to the Gulf of Genoa (Figure 15a). This high precipitable water probably fed most of the storms that developed close to the Balearic Islands and propagated toward the Alps. The simulations broadly agreed in the location of this strip of moisture but differed in quantity. ALA overestimated and ARP and ECM underestimated by a few millimeters with respect to the SSM/I retrieval. An area of positive CAPE was also associated with the strip of moisture. Values of CAPE larger than  $400 \text{ J kg}^{-1}$  were more often found in ALA than in the two other simulations which is consistent with the greater precipitable water and resulting convective activity simulated by ALA.

[54] A second area where values of precipitable water were greater than 27 mm, spread from the Balearic Islands to the Costa Brava (the coast to the northeast of Barcelona). This is where the storm leading to the large quantity of precipitation in the CEV subdomain (Figure 6a) developed. All the simulations underestimated that amount by a few millimeters with ARP giving the lowest estimation. The two other simulations differ more in CAPE, with ALA giving more unstable conditions than ECM. This is consistent with the large convective activity forecasted by ALA (Figure 14). This result suggests that a few millimeters difference in the amount of precipitable water, and errors in its location are crucial for an accurate forecast of convection over the sea.

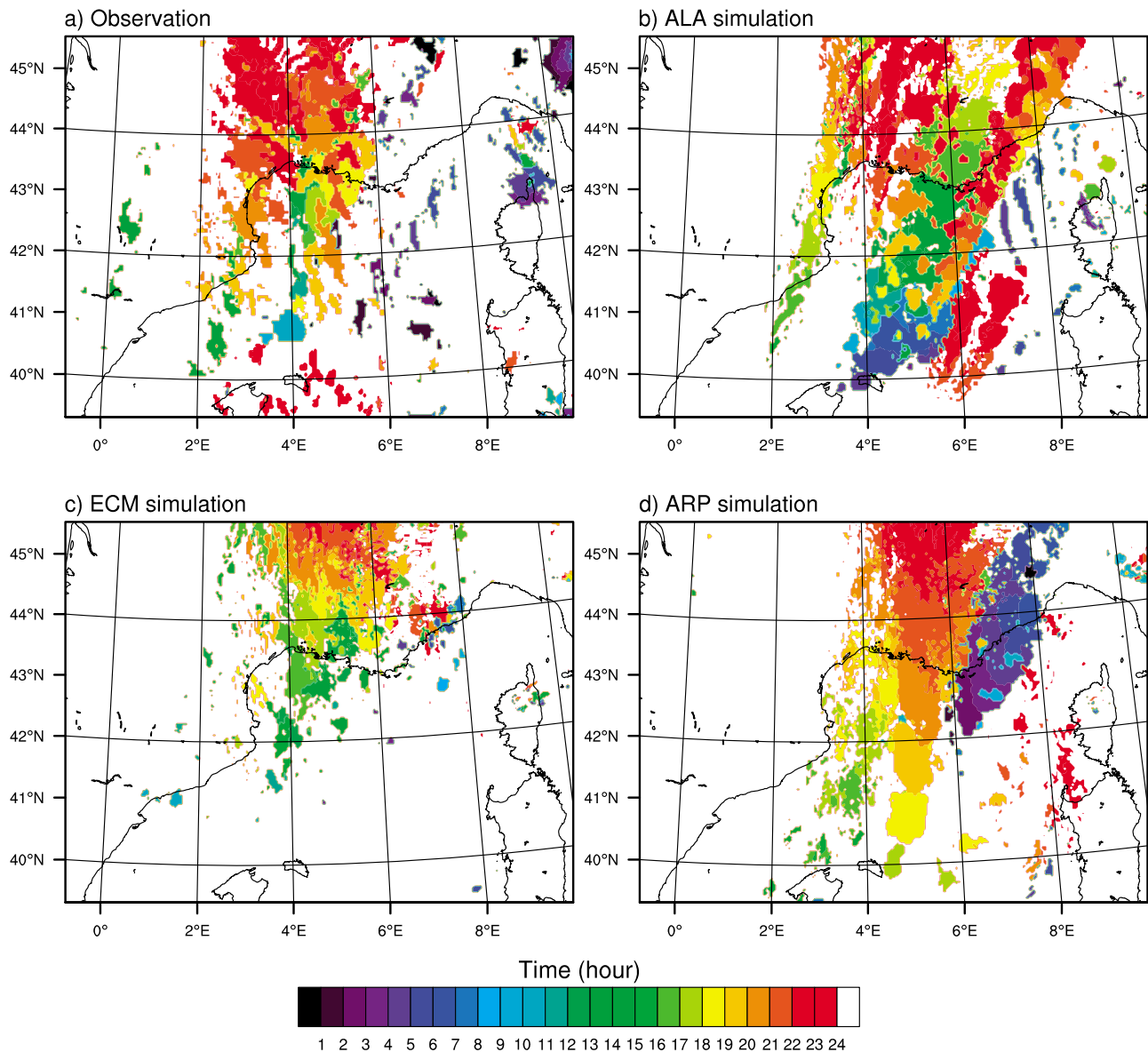


**Figure 14.** Time (hour) associated with  $10.8 \mu\text{m}$  BT less than 225 K from 0000 to 2300 UTC 22 November 2007 for (a) MSG observation and (b) ALA, (c) ECM, and (d) ARP simulations.

This was of importance in predicting heavy precipitation over the Cevennes in this particular case study.

#### 4.5. Sensitivity to Initial Conditions

[55] Much of the better performance of the ALA forecast compared with ECM and ARP forecasts can be attributed to the configuration of ALA. We illustrate this with two further experiments, ecALA and arALA, that used the ECMWF and ARPEGE analyses respectively, as initial conditions on the inner domain (rather than the outer as for ARP and ECM), and the same boundary conditions as for ALA. The resulting 3-hourly precipitation fields over the two subdomains for ecALA, arALA and ALA simulations are shown in Figure 16. On 20, 21, 22, and 23 November, the simulations differ significantly (a few millimeters) in the first 6 h accumulated precipitation. For example, 4.5 mm were observed in the CEV subdomain at 0300 UTC on 21 November, and ecALA

forecasted 6.9 mm, ecARP 4.4 and ALA 2.2. Over the same area, ECM forecasted 7.7 mm and ARP 4.9 mm. This result shows the strong impact of the initial conditions on the precipitation forecasts during the first hours of simulation. When examining the last 12 h of each simulation, the spread in the accumulated precipitation between ecALA, arALA and ALA is reduced when compared with the original experiments ECM, ARP, and ALA. For example, 12.6 mm was measured over the CEV subdomain at 0000 UTC on 23 November, ECM forecasted 2.4 mm and ARP 0.6 mm. In contrast, ecALA forecasted 9.1 mm., arALA 7.3 mm and ALA 8.3 mm. This result suggests that the impact of the boundary conditions on the precipitation forecast is substantial in the second half of the day and is particularly true during the stratiform regime as the ecALA, arALA and ALA simulations differed by less than 1 mm on 20 November.

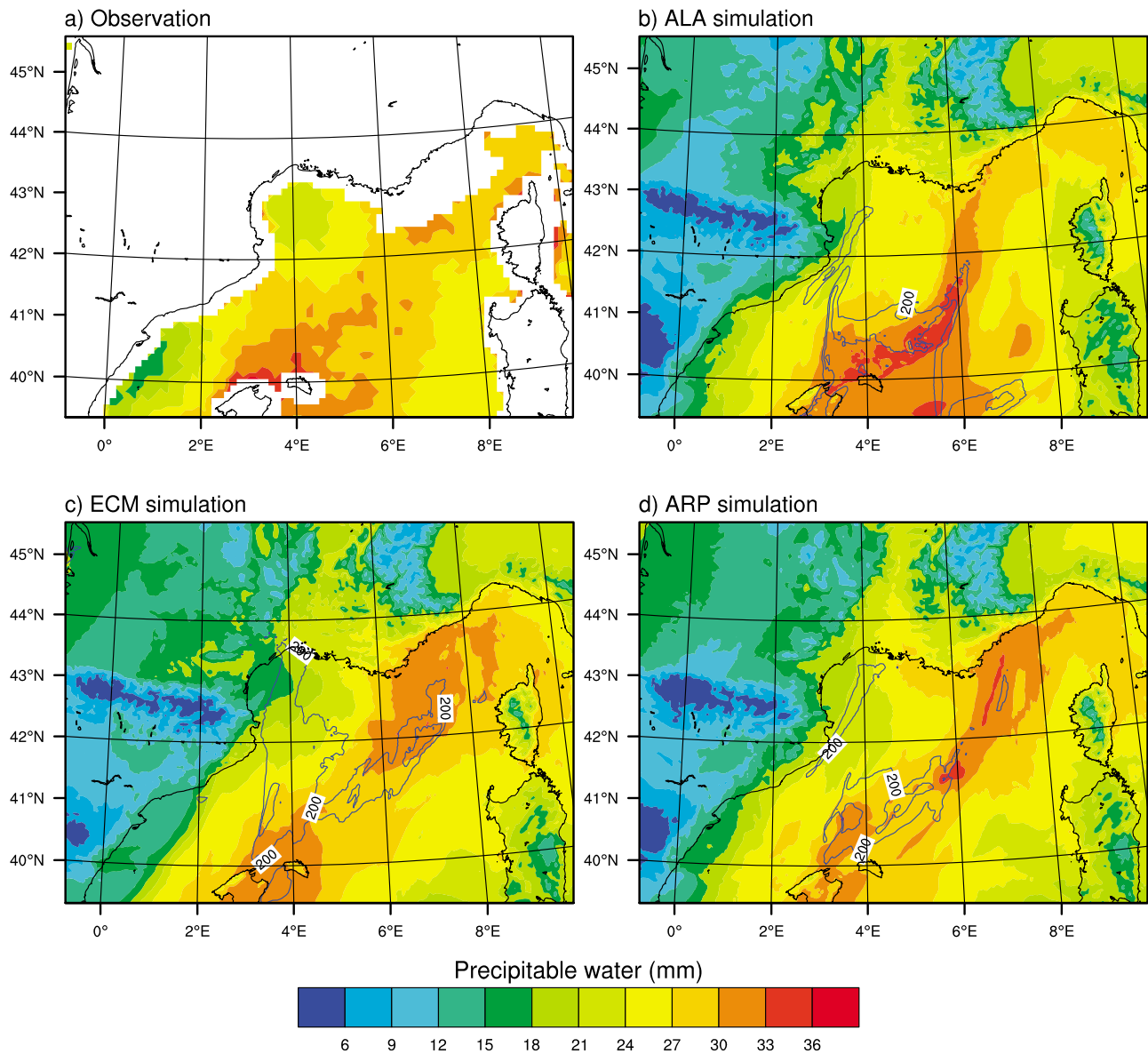


**Figure 15.** Precipitable water (mm) at 0700 UTC 22 November 2007 from (a) SSM/I observation and (b) ALA, (c) ECM, and (d) ARP simulations. In Figures 15b, 15c, and 15d the blue line represents the CAPE at 200 and 400 J kg<sup>-1</sup>.

[56] Finally, we assessed whether an improvement in the oceanic conditions would lead to a better forecast. The Mediterranean Sea supplies heat and moisture to the atmospheric boundary layer through the turbulent sea fluxes. In the Meso-NH simulations shown previously, the Sea Surface Temperature (SST) was taken from the different operational analyses and was kept constant during the 24 h forecast. It is therefore interesting to examine the sensitivity of the precipitation forecast to different oceanic conditions while keeping the atmospheric conditions unchanged. The atmospheric conditions were taken from the ALADIN analyses, as they resulted in the best forecasts. Similarly to *Lebeaupin Brossier et al.* [2008], we experimented with the use of a different set of oceanic surface conditions taken from the operational MERCATOR analyses together with the running of the one-dimensional ocean model of *Gaspar et al.* [1990].

We ran an additional set of 24 h simulations called OLA which were coupled with fields from ALADIN. The result for the precipitation is shown for the CEV subdomain only in Figure 17 as no sensitivity was found for the ALP subdomain.

[57] The range of variability during the 5 day period is small for the mean SSTs, 0.6 K for ALA and 1.1 K for ALA. At 0300 UTC (i.e., at  $t + 3$  close to the initial time) the SSTs from two sets differ up to 0.9 K on 20 November. This is within the range of errors in SST analyses found by *Lebeaupin et al.* [2006]. The SST for OLA reduces by up to 0.5 K for each 24 h simulation, the cooling was twice as much than that obtained by *Lebeaupin et al.* [2006]. Even with different initial values and temporal evolution of SST, the average sensible heat fluxes are very similar between the two sets of simulations. A larger impact of SST was on the latent heat fluxes on 20 November. The OLA oceanic fluxes

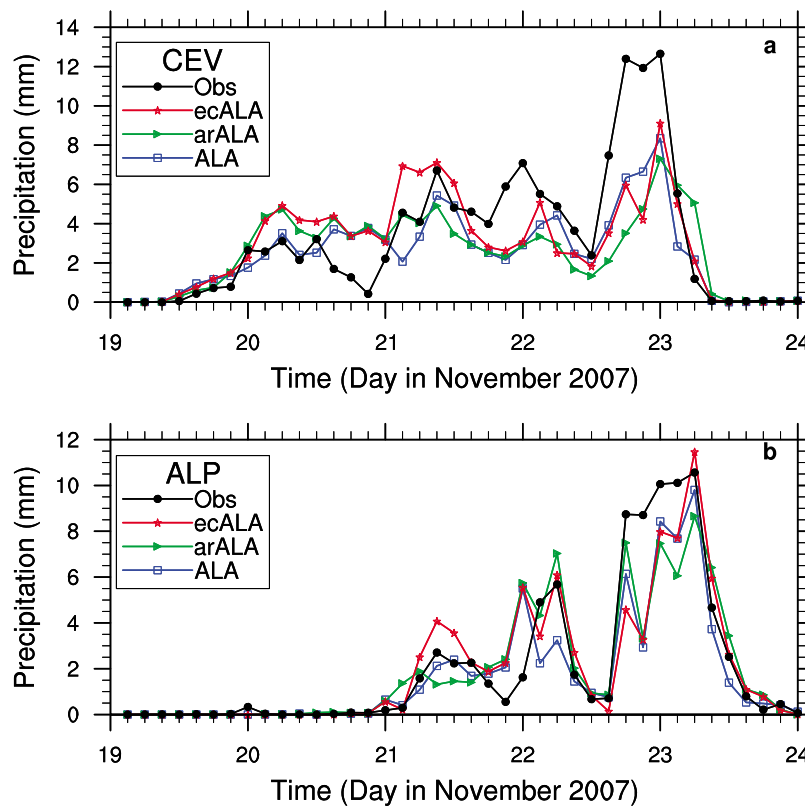


**Figure 16.** Same as Figure 6 but for ecALA, arALA, and ALA simulations.

were higher by  $10 \text{ W m}^{-2}$  compared with ALA. In consequence, together with an higher SST at initial time, the precipitation increased by about 1 mm (the average precipitation is shown over the CEV subdomain to highlight the change in amount). This increase, however, was small and we conclude that the oceanic conditions have little impact on the precipitation forecast over the Cevennes.

## 5. Conclusions

[58] A heavy precipitation event has been studied by combining rain gauge measurements, radiosoundings, satellite observations and mesoscale simulations. The event affected southeastern France from 19 to 23 November 2007. Although this was not an event of extreme precipitation for the Mediterranean (426 mm accumulated over the Cevennes) it was unusual in terms of its duration. An upper-level trough was present for the 5 days of the event and was particularly pronounced on the 22 November when the highest precipitation was experienced in the Cevennes (160 mm in 24 h). This, combined with moist boundary layer air, elevated CAPE and southerly flow was typical of a “Cevenole” episode. The Cevenole episode became more widespread on 22 November when it affected a large area of southeastern France. Satellite observations from SSM/I, AMSU and MSG confirmed the more convective scenario on 22 November compared with previous days in the event that were characterized by stratiform precipitation.

[59] Several sets of Meso-NH simulations, ECM, ARP, and ALA, were performed in order to examine the sensitivity

of precipitation forecasts to initial and boundary conditions given by ECMWF, ARPEGE and ALADIN models, respectively. These simulations were assessed against rain gauge measurements, radiosoundings and satellite observations, the latter offering a unique way to verify the performance of the forecast over the sea.

[60] On the synoptic scale, simulated precipitable water and UTH were well correlated with satellite observations and showed only small biases. The 24 h accumulated precipitation was reasonably well predicted along with the locations of the heaviest precipitation over the Cevennes and the Alps. These good agreements were obtained because of the major role of the orographic forcing in localizing precipitation.

[61] At the 3 h time scale, Meso-NH had problems predicting the correct quantity of precipitation in the catchment at a given time. While the model generally overestimated the accumulated precipitation when it was not too heavy, the quantity of precipitation was underpredicted on days characterized by intense convection and heavy precipitation. Radiosoundings gave some insights in the failures of the forecast but satellite observations allowed us to identify clearly the reasons for these discrepancies.

[62] On 20 November, a widespread layer of humid air was orographically lifted by the Cevennes resulting in sustained stratiform precipitation on the foothills of the Cevennes. ECM and ARP overestimated the quantity of precipitation on this day. Using SSM/I observations of surface wind speed we ascertained that the overestimation of precipitation was due to an overestimation of the wind speed in the Gulf of Lions where the low-level flow converged. Thus the most

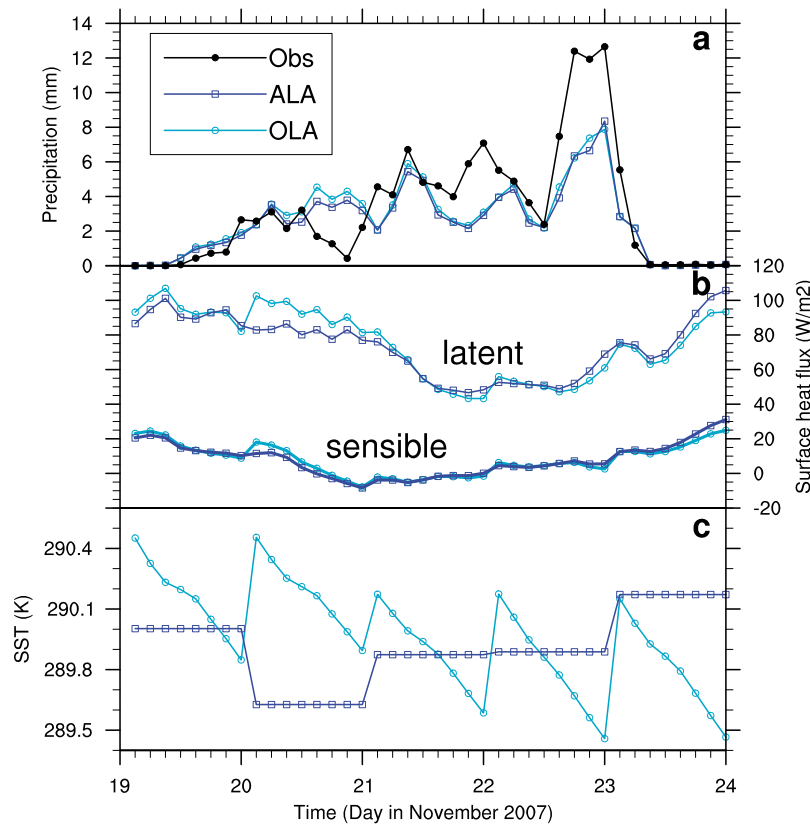


**Figure 17.** Time series of (a) 3 h accumulated precipitation ( $\text{mm h}^{-1}$ ), (b) sensible and latent heat flux at the surface ( $\text{W m}^{-2}$ ), and (c) sea surface wind temperature (K). Averages were calculated over the CEV subdomain for the 3 h accumulated precipitation and over the sea part of the inner model domain for surface heat fluxes and SST. Results are shown for ALA and OLA simulations. Outputs from each 24 h simulation are every 3 h from  $t + 3$  to  $t + 24$ .

successful simulation (ALA) was the one that gave the best simulation of wind speed.

[63] On 22 November, the underestimation of precipitation was due to the failure of the model to predict convective storms accurately. From MSG observations, we could see that these storms developed over the Balearic Islands and moved northward toward the French Mediterranean coast. The mesoscale model failed to capture the intensity of these storms and made some errors in their localization and time of onset. The heaviest precipitation was thus underpredicted by the model. SSM/I observations further suggested that the mislocation in the propagation of thunderstorms was related to an underestimation of the precipitable water over the sea.

[64] The present study also highlighted a significant sensitivity of the forecast of precipitation at the mesoscale to the configuration of the model and to the initial and boundary conditions. The simulations improved in both cases when initialized and coupled with the mesoscale ALADIN fields rather than being driven by the global assimilation systems, ECMWF or ARPEGE. In agreement with *Ducrocq et al.* [2002] and *Argence et al.* [2008] among others, our sensitivity experiments showed that the initial conditions had an impact on the forecast of precipitation during the first few hours of simulation. As *Lebeaupin et al.* [2006] and *Lebeaupin Brossier et al.* [2008] found, changes in oceanic conditions however, did not lead to a better forecast. The uncertainties

from the slow component of the ocean-atmosphere did not appear have a large impact on short-term forecasts of heavy precipitation events.

[65] As satellite observations were able to identify the sources of uncertainties in the model, their assimilation at the mesoscale should lead to an improvement in the forecasted precipitation. Indeed, the difference in initial and boundary conditions that led to different forecasts were mostly on the scale of the observations used by the assimilation in NWP systems. Radiosondes, surface observations, buoys, ship and aircraft measurements, wind profilers, horizontal winds from atmospheric motion vectors and scatterometers, and radiances from sounders are common to these systems. In ALADIN, the same observations as in ARPEGE are used, with the addition of SEVIRI radiances and of surface measurements [*Montmerle et al.*, 2007]. More satellite data were assimilated in the ECMWF system, including the cloud and rain-affected SSM/I radiances (using a two-step approach that assimilates retrieved precipitable water [*Bauer et al.*, 2006]). However, the structure functions are at a finer scale for ALADIN compared with the global models and as a result, ALA experiments initialized with ALADIN fields show the best skill at forecasting precipitation. The ALA simulations were coupled with ALADIN fields at the borders of the inner model making these simulations much more dependent on the lateral coupling than the two

other sets of simulations, and contribute to the better success of the ALA experiments.

[66] The satellite observations allowed us to characterize episodes of stratiform and convective precipitation and to identify the discrepancies in the forecasted precipitation. This is the only method that can be used over sea in a systematic way and will be used extensively for verifying forecasts during the future HyMeX (Hydrological Cycle in the Mediterranean eXperiment) field campaign (<http://www.cnrm.meteo.fr/hymex/>). Lastly, the present study supports the need to collect high-resolution data in areas upstream of the Mediterranean.

[67] **Acknowledgments.** This study was sponsored by the CYMENT project of the RTRA STAE Toulouse. We thank Météo-France for the precipitation data used in this study. Computer resources were allocated by IDRIS. MSG observations were obtained from SATMOS. AMSU data was obtained through the French Mixed Service Unit ICARE. SSM/I data come from the NOAA's Comprehensive Large Array-data Stewardship System.

## References

- Argence, S., D. Lambert, E. Richard, J.-P. Chaboureau, and N. Söhne (2008), Impact of initial conditions uncertainties on the predictability of heavy rainfall in the Mediterranean: A case study, *Q. J. R. Meteorol. Soc.*, *134*, 1775–1788.
- Argence, S., D. Lambert, E. Richard, J.-P. Chaboureau, P. Arbogast, and K. Maynard (2009), Improving the numerical prediction of a cyclone in the Mediterranean by local potential vorticity modifications, *Q. J. R. Meteorol. Soc.*, *135*, 865–879.
- Bauer, P., P. Lopez, A. Benedetti, D. Salmond, and E. Moreau (2006), Implementation of 1D+4DVar assimilation of precipitation-affected microwave radiances at ECMWF. I: 1D-Var, *Q. J. R. Meteorol. Soc.*, *132*, 2277–2306.
- Bechtold, P., E. Bazile, F. Guichard, P. Mascart, and E. Richard (2001), A mass flux convection scheme for regional and global models, *Q. J. R. Meteorol. Soc.*, *127*, 869–886.
- Belamari, S. (2005), Report on uncertainty estimates of an optimal bulk formulation for surface turbulent fluxes, *MERSEA-WP04-MF-STR-003*, MERSEA, Plouzané, France.
- Buehler, S. A., and V. O. John (2005), A simple method to relate microwave radiances to upper tropospheric humidity, *J. Geophys. Res.*, *110*, D02110, doi:10.1029/2004JD005111.
- Chaboureau, J.-P., and P. Bechtold (2002), A simple cloud parameterization derived from cloud resolving model data: diagnostic and prognostic applications, *J. Atmos. Sci.*, *59*, 2362–2372.
- Chaboureau, J.-P., and P. Bechtold (2005), Statistical representation of clouds in a regional model and the impact on the diurnal cycle of convection during Tropical Convection, Cirrus and Nitrogen Oxides (TROCCINOX), *J. Geophys. Res.*, *110*, D17103, doi:10.1029/2004JD005645.
- Chaboureau, J.-P., and C. Claud (2006), Satellite-based climatology of Mediterranean cloud systems and their association with large-scale circulation, *J. Geophys. Res.*, *111*, D01102, doi:10.1029/2005JD006460.
- Chaboureau, J.-P., and J.-P. Pinty (2006), Validation of a cirrus parameterization with Meteosat Second Generation observations, *Geophys. Res. Lett.*, *33*, L03815, doi:10.1029/2005GL024725.
- Chaboureau, J.-P., J.-P. Cammas, P. Mascart, J.-P. Pinty, C. Claud, R. Roca, and J.-J. Morcrette (2000), Evaluation of a cloud system life-cycle simulated by Meso-NH during FASTEX using METEOSAT radiances and TOVS-31 cloud retrievals, *Q. J. R. Meteorol. Soc.*, *126*, 1735–1750.
- Chaboureau, J.-P., J.-P. Cammas, P. Mascart, J.-P. Pinty, and J.-P. Lafore (2002), Mesoscale model cloud scheme assessment using satellite observations, *J. Geophys. Res.*, *107*(D16), 4301, doi:10.1029/2001JD000714.
- Chaboureau, J.-P., N. Söhne, J.-P. Pinty, I. Meirold-Mautner, E. Defer, C. Prigent, J.-R. Pardo, M. Mech, and S. Crewell (2008), A midlatitude cloud database validated with satellite observations, *J. Appl. Meteorol. Climatol.*, *47*, 1337–1353.
- Cuxart, J., P. Bougeault, and J.-L. Redelsperger (2000), A turbulence scheme allowing for mesoscale and large-eddy simulations, *Q. J. R. Meteorol. Soc.*, *126*, 1–30.
- Delrieu, G., et al. (2005), The catastrophic flash-flood event of 8–9 September 2002 in the Gard region, France: A first case study for the Cevennes-Vivarais Mediterranean Hydrometeorological Observatory, *J. Hydro-meteorol.*, *6*, 34–52.
- Ducrocq, V., D. Ricard, J.-P. Lafore, and F. Orain (2002), Storm-scale numerical rainfall prediction for five precipitating events over France: On the importance of the initial humidity field, *Weather Forecasting*, *17*, 1236–1256.
- Ducrocq, V., O. Nuissier, D. Ricard, C. Lebeaupin, and T. Thouvenin (2008), A numerical study of three catastrophic precipitating events over southern France. II: Mesoscale triggering and stationarity factors, *Q. J. R. Meteorol. Soc.*, *134*, 131–145.
- Faccani, C., D. Cimini, F. S. Marzano, and R. Ferretti (2005), Three-dimensional variational assimilation of Special Sensor Microwave/Imager data into a mesoscale weather-prediction model: A case study, *Q. J. R. Meteorol. Soc.*, *133*, 1295–1307.
- Fischer, C., T. Montmerle, L. Berre, L. Auger, and S. E. Stefanescu (2005), An overview of the variational assimilation in the ALADIN/France numerical weather-prediction system, *Q. J. R. Meteorol. Soc.*, *131*, 3477–3492.
- Funatsu, B. M., C. Claud, and J.-P. Chaboureau (2007), Potential of Advanced Microwave Sounding Unit to identify precipitating systems and associated upper-level features in the Mediterranean region: Case studies, *J. Geophys. Res.*, *112*, D17113, doi:10.1029/2006JD008297.
- Funatsu, B. M., C. Claud, and J.-P. Chaboureau (2008), A 6-year AMSU-based climatology of stratospheric intrusions and associated precipitation distribution in the Mediterranean region, *J. Geophys. Res.*, *113*, D15120, doi:10.1029/2008JD009918.
- Funatsu, B. M., C. Claud, and J.-P. Chaboureau (2009), Comparison between the large-scale environment of moderate and intense precipitating systems in the Mediterranean region, *Mon. Weather Rev.*, *137*, 3933–3959.
- Gaspar, P., Y. Grégoris, and J.-M. Lefevre (1990), A simple eddy kinetic energy model for simulations of the oceanic vertical mixing: Tests at station Papa and long-term upper ocean study site, *J. Geophys. Res.*, *95*(C9), 16,179–16,193, doi:10.1029/JC095iC09p16179.
- Goodberlet, M., C. Swift, and J. Wilkerson (1989), Remote sensing of ocean surface winds with the Special Sensor Microwave/Imager, *J. Geophys. Res.*, *94*(C10), 14,547–14,555, doi:10.1029/JC094iC10p14547.
- Gregory, D., J.-J. Morcrette, C. Jakob, A. M. Beljaars, and T. Stockdale (2000), Revision of convection, radiation and cloud schemes in the ECMWF model, *Q. J. R. Meteorol. Soc.*, *126*, 1685–1710.
- Hoinka, K. P., C. Schwierz, and O. Martius (2006), Synoptic-scale weather patterns during Alpine heavy rain events, *Q. J. R. Meteorol. Soc.*, *132*, 2853–2860.
- Hong, G., G. Heygster, J. Miao, and K. Kunzi (2005), Detection of tropical deep convective clouds from AMSU-B water vapor channels measurements, *J. Geophys. Res.*, *110*, D05205, doi:10.1029/2004JD004949.
- Kummerow, C., and L. Giglio (1994), A passive microwave technique for estimating rainfall and vertical structure information from space. Part I: Algorithm description, *J. Appl. Meteorol.*, *33*, 3–18.
- Lafore, J.-P., et al. (1998), The Meso-NH Atmospheric Simulation System. Part I: Adiabatic formulation and control simulations: Scientific objectives and experimental design, *Ann. Geophys.*, *16*, 90–109.
- Lagouvardos, K., and V. Kotroni (2005), Improvement of high-resolution weather forecasts through humidity adjustment based on satellite data, *Q. J. R. Meteorol. Soc.*, *131*, 1519–1531.
- Lebeaupin, C., V. Ducrocq, and H. Giordani (2006), Sensitivity of Mediterranean torrential rain events to the sea surface temperature based on high-resolution numerical forecasts, *J. Geophys. Res.*, *111*, D12110, doi:10.1029/2005JD006541.
- Lebeaupin Brossier, C., V. Ducrocq, and H. Giordani (2008), Sensitivity of three Mediterranean heavy rain events to two different sea surface fluxes parameterizations in high-resolution numerical modeling, *J. Geophys. Res.*, *113*, D21109, doi:10.1029/2007JD009613.
- Mlawer, E. J., S. J. Taubman, P. D. Brown, M. J. Iacono, and S. A. Clough (1997), Radiative transfer for inhomogeneous atmospheres: RRTM, a validated correlated-k model for the longwave, *J. Geophys. Res.*, *102*(D14), 16,663–16,682, doi:10.1029/97JD00237.
- Montmerle, T., F. Rabier, and C. Fischer (2007), Relative impact of polar-orbiting and geostationary satellite radiances in the Aladin/France numerical weather prediction system, *Q. J. R. Meteorol. Soc.*, *133*, 655–671.
- Morcrette, J.-J. (1991), Evaluation of model-generated cloudiness: Satellite-observed and model-generated diurnal variability of brightness temperature, *Mon. Weather Rev.*, *119*, 1205–1224.
- Noilhan, J., and S. Planton (1989), A simple parameterization of land surface processes for meteorological models, *Mon. Weather Rev.*, *117*, 536–549.
- Nuissier, O., V. Ducrocq, D. Ricard, C. Lebeaupin, and S. Anquetin (2008), A numerical study of three catastrophic precipitating events over southern France. I: Numerical framework and synoptic ingredients, *Q. J. R. Meteorol. Soc.*, *134*, 111–130.

- Pergaud, J., V. Masson, S. Malardel, and F. Couvreur (2009), A parameterization of dry thermals and shallow cumuli for mesoscale numerical weather prediction, *Boundary Layer Meteorol.*, *132*, 83–106.
- Petty, G. W. (1994), Physical retrievals of over-ocean rain rate from multichannel microwave imagery. Part II: Algorithm implementation, *Meteorol. Atmos. Phys.*, *54*, 101–122.
- Pinty, J.-P., and P. Jabouille (1998), A mixed-phase cloud parameterization for use in a mesoscale non-hydrostatic model: Simulations of a squall line and of orographic precipitations, paper presented at Conference on Cloud Physics, Am. Meteorol. Soc., Everett, Wash.
- Richard, E., A. Buzzi, and G. Zängl (2007), Quantitative precipitation forecasting in the Alps: The advances achieved by the Mesoscale Alpine Programme, *Q. J. R. Meteorol. Soc.*, *133*, 831–846.
- Romero, R. (2001), Sensitivity of a heavy rain producing western Mediterranean cyclone to embedded potential vorticities anomalies, *Q. J. R. Meteorol. Soc.*, *127*, 2559–2597.
- Saunders, R., M. Matricardi, P. Brunel, S. English, P. Bauer, U. O’Keeffe, P. Francis, and P. Rayer (2005), RTTOV-8 Science and validation report, *NWPSAF-MO-TV-007*, 41 pp., Met Off., Exeter, U. K.
- Söhne, N., J.-P. Chaboureau, and F. Guichard (2008), Verification of cloud cover forecast with satellite observation over West Africa, *Mon. Weather Rev.*, *136*, 4421–4434.
- Stein, J., E. Richard, J.-P. Lafore, J.-P. Pinty, N. Asencio, and S. Cosma (2000), High-resolution non-hydrostatic simulations of flash-flood episodes with grid-nesting and ice-phase parameterization, *Meteorol. Atmos. Phys.*, *72*, 203–221.

---

J.-P. Chaboureau and H. Clark, Laboratoire d’Aerologie, Observatoire Midi-Pyrénées, 14 av. Belin, F-31400 Toulouse, France. (jean-pierre.chaboureau@aero.obs-mip.fr; hannah.clark@aero.obs-mip.fr)